Human SFI1 and Centrin form a complex critical for centriole architecture and ciliogenesis

Marine Laporte, Imène Bouhlel, Eloïse Bertiaux, Ciaran Morrison, Alexia Giroud, Susanne Borgers, Juliette Azimzadeh, Michel Bornens, Paul Guichard, Anne Paoletti, et al.

Human SFI1 and Centrin form a complex critical for centriole architecture and ciliogenesis

Marine H Laporte[1],[†] [ID], Imène B Bouhlel[2],[†], Eloïse Bertiaux[1], Ciaran G Morrison[1],[3] [ID], Alexia Giroud[1] [ID], Susanne Borgers[1], Juliette Azimzadeh[4], Michel Bornens[2],[‡], Paul Guichard[1],[*] [ID], Anne Paoletti[2],[**] [ID] & Virginie Hamel[1],[***] [ID]

Abstract

Over the course of evolution, the centrosome function has been conserved in most eukaryotes, but its core architecture has evolved differently in some clades, with the presence of centrioles in humans and a spindle pole body (SPB) in yeast. Similarly, the composition of these two core elements has diverged, with the exception of Centrin and SFI1, which form a complex in yeast to initiate SPB duplication. However, it remains unclear whether this complex exists at centrioles and whether its function has been conserved. Here, using expansion microscopy, we demonstrate that human SFI1 is a centriolar protein that associates with a pool of Centrin at the distal end of the centriole. We also find that both proteins are recruited early during procentriole assembly and that depletion of SFI1 results in the loss of the distal pool of Centrin, without altering centriole duplication. Instead, we show that SFI1/Centrin complex is essential for centriolar architecture, CEP164 distribution, and CP110 removal during ciliogenesis. Together, our work reveals a conserved SFI1/Centrin module displaying divergent functions between mammals and yeast.

Introduction

Centrosomes are membrane-less organelles, originally discovered by Theodor Boveri over a hundred years ago, which perform essential functions in processes such as cell division (Boveri, 1900; Bornens, 2012). In this case, centrosomes function as the main microtubule nucleating center of the cell (MTOC), forming the two poles of the mitotic spindle that segregates the genetic material equally into the two daughter cells.

While the centrosome is conserved in functional terms in almost all higher eukaryotes, excepted in seed plants, its structure, revealed by numerous electron microscopy studies, has diverged throughout evolution in some species (Azimzadeh, 2014; Ito & Bettencourt-Dias, 2018). In most eukaryotes, such as mammals, the centrosome is a proteinaceous condensate surrounding two highly sophisticated core elements called centrioles. Centrioles are 450 nm long cylindrical structures made of nine microtubule triplets (LeGuennec et al, 2021), which duplicate in a conservative manner once per cell cycle, during the S phase (Azimzadeh & Marshall, 2010). In some species, such as yeast or *Dictyostelium*, centrioles have been lost during evolution and replaced by smaller protein assemblies that retain duplication and microtubule nucleation capabilities (Azimzadeh, 2014; Ito & Bettencourt-Dias, 2018; Nabais et al, 2020). In yeast, the centrosome is called the spindle pole body (SPB) and is composed of a core element made of outer and inner plaques associated with a side appendage, the half-bridge, which controls its duplication (Seybold & Schiebel, 2013; Kilmartin, 2014).

In agreement with the large structural diversity of centrosomes between species, the proteins that constitute their core elements have also diverged greatly (Hodges et al, 2010; Carvalho-Santos et al, 2011; Ito & Bettencourt-Dias, 2018; Nabais et al, 2020). As an illustration, the evolutionarily conserved proteins SAS-6, SAS-4/CPAP, CEP135/Bld10p, and POC1, all critical for centriole duplication and assembly, are absent in yeast (Carvalho-Santos et al, 2011). More generally, even though some centrosome proteins have been conserved between mammals and yeast, only Centrins have been clearly characterized as being present in both centrioles and yeast SPBs. In mammals, four Centrins, Centrin 1 to Centrin 4 have

1 Department of Molecular and Cellular Biology, University of Geneva, Geneva, Switzerland
2 Institut Curie, UMR 144, CNRS, PSL University, Paris, France
3 Centre for Chromosome Biology, School of Biological and Chemical Sciences, National University of Ireland Galway, Galway, Ireland
4 Université Paris Cité, CNRS, Institut Jacques Monod, Paris, France
   *Corresponding author. Tel: +41 22 379 67 50; E-mail: paul.guichard@unige.ch
   **Corresponding author. Tel: +33 1 56 24 68 12; E-mail: anne.paoletti@curie.fr
   ***Corresponding author. Tel: +41 22 379 67 35; E-mail: virginie.hamel@unige.ch
   †These authors contributed equally to this work
   ‡Deceased

been identified (Salisbury *et al*, 1984; Middendorp *et al*, 1997; Gavet *et al*, 2003; Bauer *et al*, 2016), with Centrin 1 expressed in the testis and in the retina (Wolfrum & Salisbury, 1998; Hart *et al*, 1999) and Centrin 4 in ciliated cells (Gavet *et al*, 2003). Centrin proteins are recruited early to procentrioles in the distal lumen of centrioles (Paoletti *et al*, 1996; Laoukili *et al*, 2000; Middendorp *et al*, 2000). Ultrastructure expansion microscopy (U-ExM), amenable to nanoscale protein mapping (Gambarotto *et al*, 2019), further revealed a dual localization for Centrin at the central core region and the very distal end of the centriole (Le Guennec *et al*, 2020; Steib *et al*, 2020). Functionally, animal Centrins are not required for centrosome duplication (Strnad *et al*, 2007; Dantas *et al*, 2011), but they are necessary for normal ciliogenesis (Dantas *et al*, 2011; Delaval *et al*, 2011; Prosser & Morrison, 2015).

Budding or fission yeasts contain only a single Centrin homolog, named Cdc31. Cdc31 is important for SPB duplication and associates with the protein Sfi1 (Baum *et al*, 1986; Vallen *et al*, 1994; Spang *et al*, 1995; Kilmartin, 2003; Paoletti *et al*, 2003; Li *et al*, 2006), an extended α-helix that possess multiple Cdc31-binding domains (Li *et al*, 2006), and which, upon Cdc31 binding, assembles into a parallel array to form the SPB half-bridge. Assembly of the second array of Sfi1/Cdc31, anti-parallel to the first and associated with it through Sfi1 C-termini, provides the site for daughter SPB assembly, thereby controlling conservative SPB duplication (Kilmartin, 2014; Bouhlel *et al*, 2015; Bestul *et al*, 2017; Rüthnick *et al*, 2021). Recently, applying U-ExM to budding yeast allowed the visualization of the Sfi1/Cdc31 core module on the half-bridge structure (preprint: Hinterndorfer *et al*, 2022).

Interestingly, it was shown that SFI1 localizes at centrosomes in human cells (Kilmartin, 2003; Kodani *et al*, 2019) and can interact directly with human Centrins *in vitro* (Martinez-Sanz *et al*, 2006, 2010). However, it remains unclear whether Centrins and human SFI1 form a complex at centrioles. Indeed, in contrast to Centrins, it was recently proposed that SFI1 regulates centriole duplication, similarly to its function at SPBs, by stabilizing the centriolar proximal end protein, STIL (Balestra *et al*, 2013; Kodani *et al*, 2019). These results raised the possibility that the SFI1/Centrin complex has not

been functionally conserved in human centrioles. To test this hypothesis, we studied the fine localization and function of human SFI1, combining cell biology and expansion microscopy techniques. We first establish that SFI1 is a molecular constituent of the centriole that co-localizes with a distinct pool of Centrin 2/3 at the very distal tip of human centrioles, from the early stages of centriole biogenesis. We further demonstrate that SFI1 is dispensable for centriole duplication but that its depletion leads to the specific loss of the distal pool of Centrins and strongly affects centriole architecture, CP110 decapping, and CEP164 distribution. These results reveal that the SFI1/Centrin complex is conserved in mammals, but also suggest that its function differs from that observed in yeast: it is not required for centriole duplication but is important to ensure the proper stability of centrioles as well as to regulate ciliogenesis.

Results

Human SFI1 is a *bona fide* centriolar component localizing at the very distal end

Human SFI1 is an evolutionarily conserved protein of 1,242 amino acids that contains about 23 characteristic SFI1 repeats (Kilmartin, 2003; Li *et al*, 2006; Appendix Fig S1). SFI1 has been shown to localize at centrosomes (Kilmartin, 2003; Kodani *et al*, 2019) as well as at centriolar satellites during S phase (Kodani *et al*, 2015). To investigate whether SFI1 is a *bona fide* centriolar component, we raised and affinity-purified a polyclonal antibody against a C-terminal fragment of the protein encompassing residues 1,021–1,240 (Appendix Fig S1). First, immunofluorescence analysis of cycling immortalized hTERT RPE-1 cells (hereafter referred to as RPE-1) co-stained for the centrosomal marker γ-tubulin and SFI1, demonstrated its localization at centrosomes throughout the cell cycle (Fig 1A). We confirmed this centriolar localization of SFI1 using co-staining with the Centrin 20H5 monoclonal antibody, which recognizes human Centrin 2 and Centrin 3 (Sanders & Salisbury, 1994; Paoletti *et al*, 1996; Middendorp *et al*, 1997; Fig 1B). To further

Figure 1. SFI1 is a centriolar protein co-localizing with Centrin 2 and 3 at the distal tip of centrioles.

A, B Representative confocal images of cycling RPE-1 cells stained for SFI1 (green) and γ-Tubulin (magenta) (A) or SFI1 (green) and Centrin 2/3 (magenta) (B). Scale bar: 5 μm. Dashed-line squares correspond to insets.

C, D Representative confocal images of expanded centrioles from RPE-1 cells stained for α/β-tubulin (αβTub, magenta) and SFI1 (green). Right panels show top view images across the centriolar length confirming the distal localization of SFI1 at centrioles. The white arrowhead indicates SFI1 distal dot at centrioles. Scale bars: 200 and 100 nm (right panels). The average position of SFI1 alongside the centriole is shown in (D).

E, F Representative confocal images of expanded centrioles from RPE-1 cells stained for α/β-tubulin (αβTub, magenta) and Centrin 2/3 (Cetn2/3, gray). Right panels show top view images across the centriolar length confirming the distal localization of Centrin 2/3 at centrioles. The white arrowhead indicates Centrin 2/3 distal dot at centrioles. Scale bars: 200 and 100 nm (right panels). The average position of Centrin 2/3 alongside the centriole is shown in (F).

G, H Representative confocal images of expanded centrioles from RPE-1 cells stained for α/β-tubulin (αβTub, magenta) and Centrin 3 (Cetn3, cyan). Right panels show top view images across the centriolar length confirming the distal localization of Centrin 3 at centrioles. The white arrowhead indicates Centrin 3 distal dot at centrioles. Scale bars: 200 and 100 nm (right panels). The average position of Centrin 3 alongside the centriole is shown in (H).

I, J Representative confocal images of expanded centrioles from RPE-1 cells stained for α/β-tubulin (αβTub, magenta), SFI1 (green), and Centrin 2/3 (Cetn3, gray). Right panels show top view images confirming the distal localization of SFI1 and Centrin 2/3 at centrioles. Scale bars: 200 and 100 nm (right panels). The average position of SFI1 and Centrin 2/3 alongside the centriole is shown in (J).

K, L Position of SFI1 and Centrin signals at the distal centriolar region in nm either from separated stainings (K) or co-stainings (L).

Data information: Average ± SD, N, statistical analysis: (D) $N = 42$ centrioles from three independent experiments. (F) $N = 26$ centrioles from three independent experiments. (H) $N = 25$ centrioles from three independent experiments. (J) $N = 54$ centrioles from three independent experiments. (K) SFI1 = 376 ± 18 nm; Centrin 2/3: 355 ± 36 nm; and Centrin 3: 359 ± 37 nm. $N = 41$, 25, and 24 centrioles for SFI1, Centrin 2/3, and Centrin 3, respectively, from two independent experiments. One-way ANOVA followed by Bonferroni *post hoc* test (SFI1 vs. Cetn2/3 $P = 0.0196$, SFI1 vs. Cetn3 $P = 0.0702$, and Cetn2/3 vs. Cetn3 $P = 0.999$). (L) SFI1 = 316.3 ± 43.8 nm and Centrin 2/3: 351.8 ± 42.6 nm. $N = 53$ centrioles from three independent experiments. Unpaired *t*-test (SFI1 vs. Cetn2/3 **$P < 0.0001$).
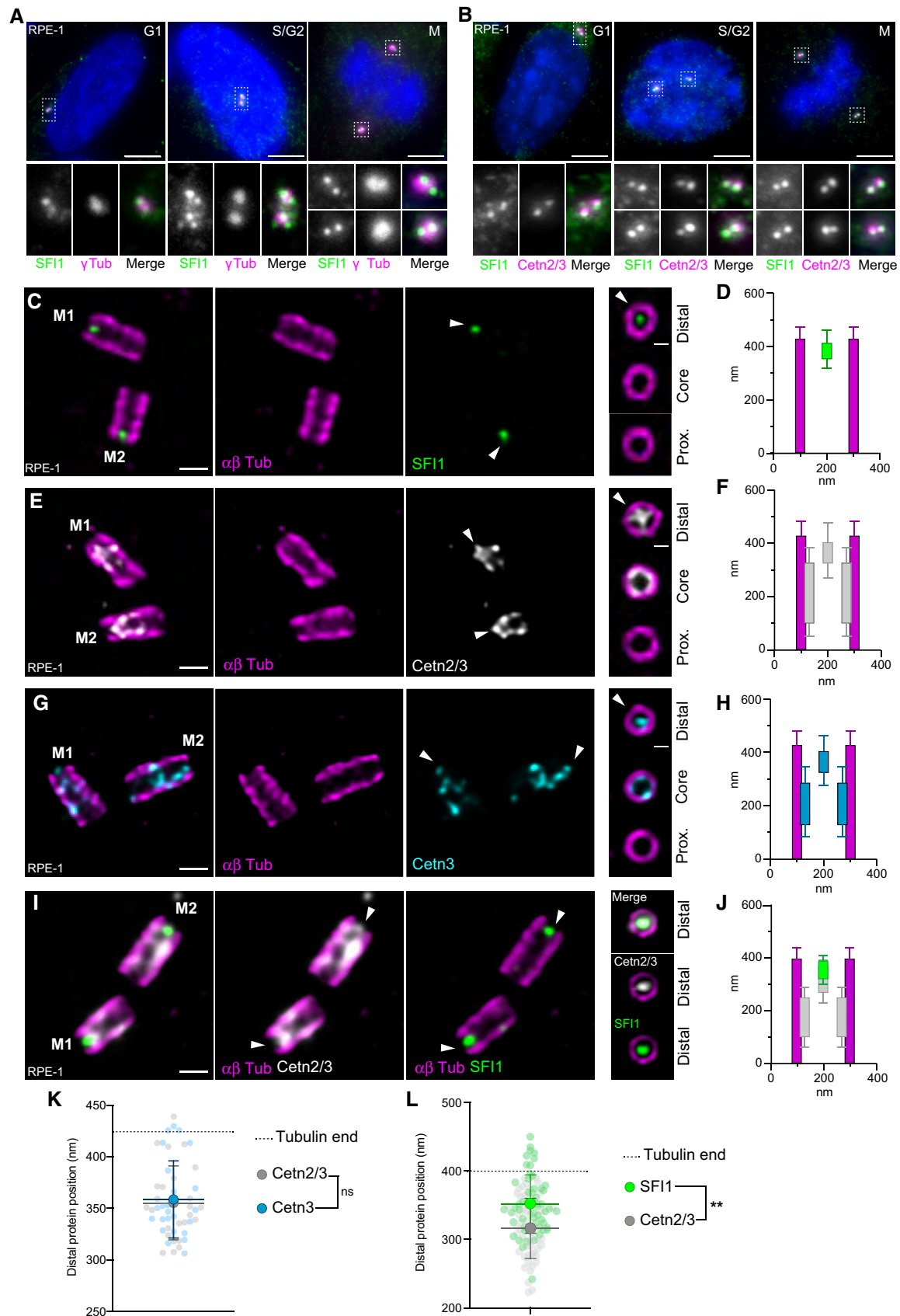
Figure 1.

investigate the precise localization of SFI1 at centrioles, we turned to super-resolution ultrastructure expansion microscopy (U-ExM; Gambarotto et al, 2019, 2021). Interestingly, we found, in two different cell lines, U2OS and RPE-1 that the C-terminus of SFI1 localizes as a distinct dot at the very distal tip in mature centrioles (Figs 1C and D, and EV1A and B). To ascertain the specificity of this signal, we analyzed SFI1 distribution in RPE-1 cells depleted of SFI1 upon siRNA treatment, as previously described (Balestra et al, 2013). We found that the distal dot corresponding to SFI1 disappeared, confirming the specificity of the signal (Fig EV1C–E). The specificity of this localization was further tested using a commercially available SFI1 antibody that targets a similar region (13550-1-AP, Proteintech Europe). We found the same localization at the distal extremity, which decreased upon siRNA depletion of SFI1 in RPE-1 cells (Fig EV1F–K). We also noted a faint, punctate proximal signal that decreased upon SFI1 depletion, possibly reflecting a putative additional location for SFI1 (Fig EV1C, D, H and J, red arrowhead).

We next compared the precise distribution of SFI1 and Centrin 2/3 at centrioles (Fig 1C–L). We first found that both Centrin 2/3 and Centrin 3 localize as a dot at the distal tip of centrioles, about 3 nm apart (Fig 1K), with additional distribution at the central core region, as previously reported (Le Guennec et al, 2020; Fig 1E–H). Given the similar localization observed with antibodies that recognize Centrin 2/3 and Centrin 3 (Fig 1K), we use "Centrin" as a generic term for both Centrin isoforms throughout the rest of the paper and specify individual isoforms as appropriate. Next, we performed triple labeling of SFI1, Centrin, and tubulin simultaneously (Fig 1I and J) and we found that SFI1 and Centrin localize at the same distal position, with SFI1 ~35 nm above Centrin (Fig 1L). Based on this nanometric proximity, and the known in vitro interaction between Centrin and SFI1 in yeast and human (Li et al, 2006; Martinez-Sanz et al, 2006; Bouhlel et al, 2015), we propose that Centrin and SFI1 form a complex at the distal end of the human centriole.

Next, we decided to monitor the recruitment of the SFI1/Centrin complex during centriole assembly. As Centrin is recruited to procentrioles during the early phases of centriole biogenesis (Paoletti et al, 1996; Middendorp et al, 1997), we investigated whether this was also the case for SFI1. Immunofluorescence analysis of RPE-1 cells in the S phase, identified using the nuclear PCNA marker (Takasaki et al, 1981), indicated the presence of more than two dots of SFI1 at centrosomes at this stage (Fig 2A), compatible with recruitment of SFI1 at procentrioles. However, the SFI1 signal appears cloudy, reminiscent of the satellite localization previously described (Kodani et al, 2015). Therefore, to improve the resolution of our microscopy, we next analyzed SFI1 localization in duplicating centrioles using U-ExM (Fig 2B). We found that SFI1 localizes at procentrioles, and, similarly to Centrin, is already present at the growing distal tip of nascent procentrioles in both RPE-1 and U2OS cells (Figs 2B and EV1A, B, F and G). This result demonstrates that the SFI1/Centrin complex is recruited at the onset of centriole biogenesis.

SFI1 is critical for distal Centrin recruitment at centrioles

Next, we assessed the impact of SFI1 depletion on Centrin localization at centrioles. To do so, we co-stained control and SFI1-depleted RPE-1 cells with antibodies against Centrin and the distal end

protein CP110 as a marker for the centriole (Schmidt et al, 2009; Fig EV2A). We found that the Centrin signal was strongly reduced upon SFI1 depletion, often solely present at one centriole, while CP110 appeared unchanged (Fig EV2A and B). To confirm this finding, we turned again to expansion microscopy, where we first monitored SFI1 depletion at centrioles. We found that 87% of cells were depleted of SFI1 at centrioles, with 52% of the centrioles within a centrosome lacking entirely the distal dot of SFI1 (No SFI1, Fig EV1L) and 35% displaying a partial depletion (Partial SFI1, Fig EV1M), meaning that at least one centriole had a remaining SFI1 dot (Fig 3A, B and G). Similarly, we observed that 82% of centrioles had lost Centrins at their distal end (Fig 3D, E and I, yellow arrowhead) while retaining the Centrin signal at the inner scaffold region (Fig 3E). This result suggests that SFI1 specifically controls the localization of a Centrin pool at the distal end of centrioles. To further strengthen this hypothesis, we depleted the inner scaffold protein POC5, which also interacts with Centrin (Azimzadeh et al, 2009) and analyzed the distribution of both Centrin and SFI1. Remarkably, we found that both SFI1 and the distal pool of Centrin remained unchanged upon POC5 depletion (Fig 3C, F, H and J). However, loss of POC5 strongly affected the pool of Centrin at the inner scaffold region (Figs 3F and EV1N–R). This observation demonstrates that Centrin forms two distinct complexes, one at the inner scaffold relying on POC5, and one at the distal end of centrioles, dependent on SFI1.

To confirm the specificity of the results obtained with SFI1 depletion and ensure that they correspond to an on-target effect, we next performed a rescue experiment by expressing SFI1 fused to mCherry, SNAP (Lukinavičius et al, 2013), or GFP. However, we found in U-ExM that even if GFP-SFI1 displayed a signal close to centrioles as previously observed (Kilmartin, 2003), none of these fusion proteins were properly localized as a distal dot at centrioles, suggesting that SFI1 tagging might be deleterious for its proper localization and function (Appendix Fig S2A). Therefore, we cloned an untagged RNAi-resistant version of SFI1 (SFI1-RR) in a pIRES-GFP plasmid, delivering SFI1-RR and GFP as separate proteins, a strategy that allowed us to monitor the transfection efficiency (Appendix Fig S2B). The expression of this construct significantly rescued the distal localization of both SFI1 and Centrin at centrioles (Fig 3K–N), indicating that the Centrin loss observed at the distal end of centrioles is specifically due to the depletion of SFI1.

Finally, we asked whether SFI1 localization would be impacted by the depletion of Centrin 2, using Centrin 2 RPE-1 knock-out cells (Cetn2 KO; Fig 3O). We found that SFI1 localization was totally lost in Cetn2 KO cells, with 96% of cells lacking the distal dot of SFI1 at centrioles (Fig 3P). We further show that SFI1 localization is restored in RPE1 Centrin 2 KO cells that stably express Centrin 2 (Khouj et al, 2019; Fig 3O and P), demonstrating that both proteins are interdependent for their localization at the distal end of centrioles.

SFI1/Centrin complex is not involved in centriole duplication

It has been reported that SFI1 depletion impacts centriole duplication (Balestra et al, 2013; Kodani et al, 2019), using the Centrin signal as a readout. Since we demonstrated that SFI1 controls the distal localization of Centrin to the centriole, we concluded that Centrin might not be an ideal marker to monitor centriole duplication per se. Therefore, we decided to re-examine the function of SFI1 in
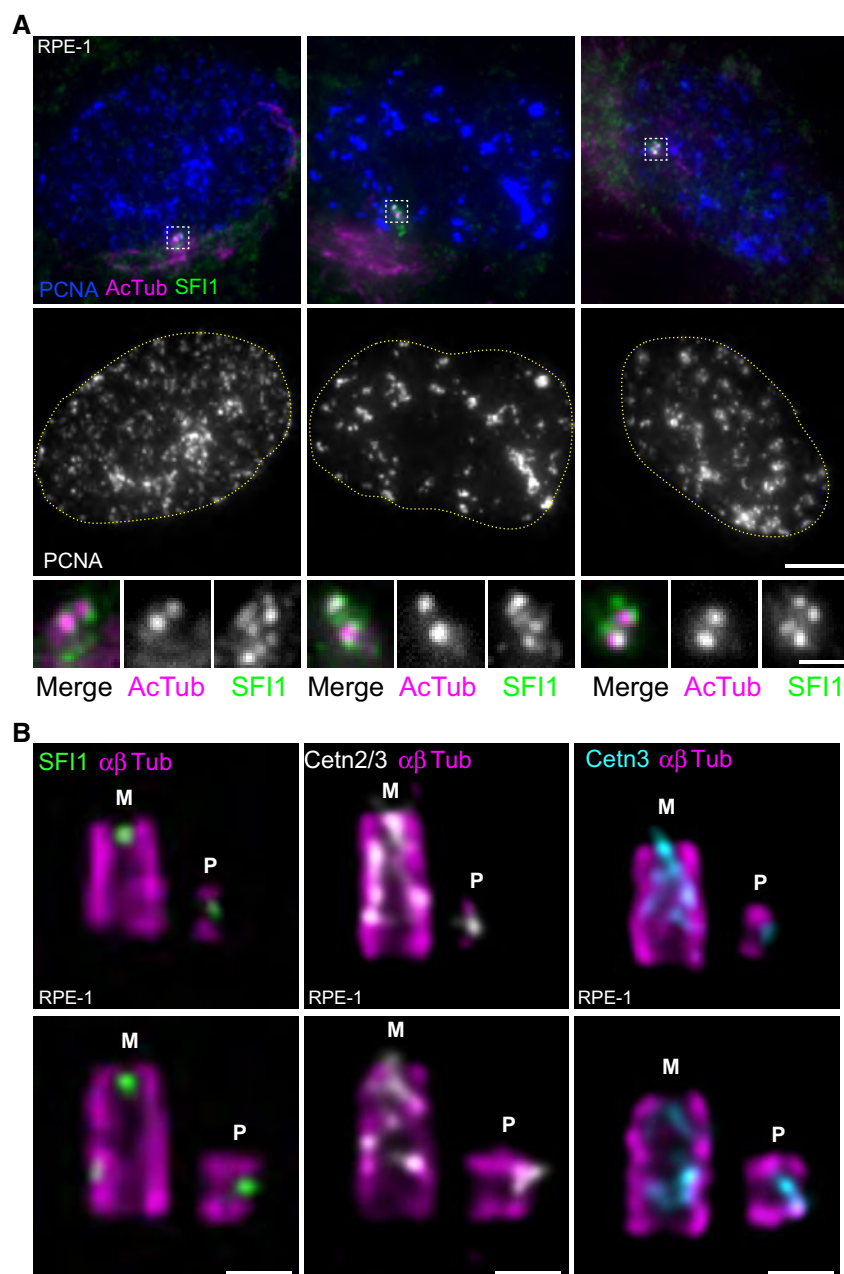
Figure 2. SFI1 and Centrin are recruited at the onset of centriole biogenesis.

A Representative confocal images of RPE-1 cycling cells stained for SFI1 (green), acetylated tubulin (AcTub, magenta), and PCNA (blue). DNA boundaries are marked with a yellow dotted line. White dashed line squares correspond to insets. Scale bar: 5 µm.

B Representative confocal images of expanded duplicating centrioles from RPE-1 cells stained for α/β-tubulin (αβTub, magenta) and SFI1 (green, left panel), Centrin 2/3 (Cetn2/3, gray, middle panel) or Centrin 3 (Cetn3, cyan, right panel). M stands for mature centriole and P stands for procentriole. Note that both SFI1 and Centrins are recruited very early at procentrioles as a distal dot. Scale bars: 200 nm.

centriole duplication. To do so, we turned to both osteosarcoma U2OS and HeLa cells, which are widely used to study centriole duplication. We could not observe any difference in the percentage of cells with procentriole between control and SFI1-depleted cells (Figs 4A–C and EV3A–D), in contrast to the strong reduction of the number of Centrin dots observed in regular immunofluorescence (Fig EV2A and B; Balestra *et al*, 2013; Kodani *et al*, 2019). To

confirm our observations, we monitored the presence of the cartwheel proteins HsSAS-6 and STIL at procentrioles, as previous data showed that SFI1-depleted HeLa cells failed to recruit these two proteins to S-phase centrosomes, probably owing to STIL destabilization (Kodani *et al*, 2019). In contrast, we found that both HsSAS-6 and STIL are properly recruited to the growing procentrioles of SFI1-depleted U2OS cells (Fig 4D and E). To further clarify the
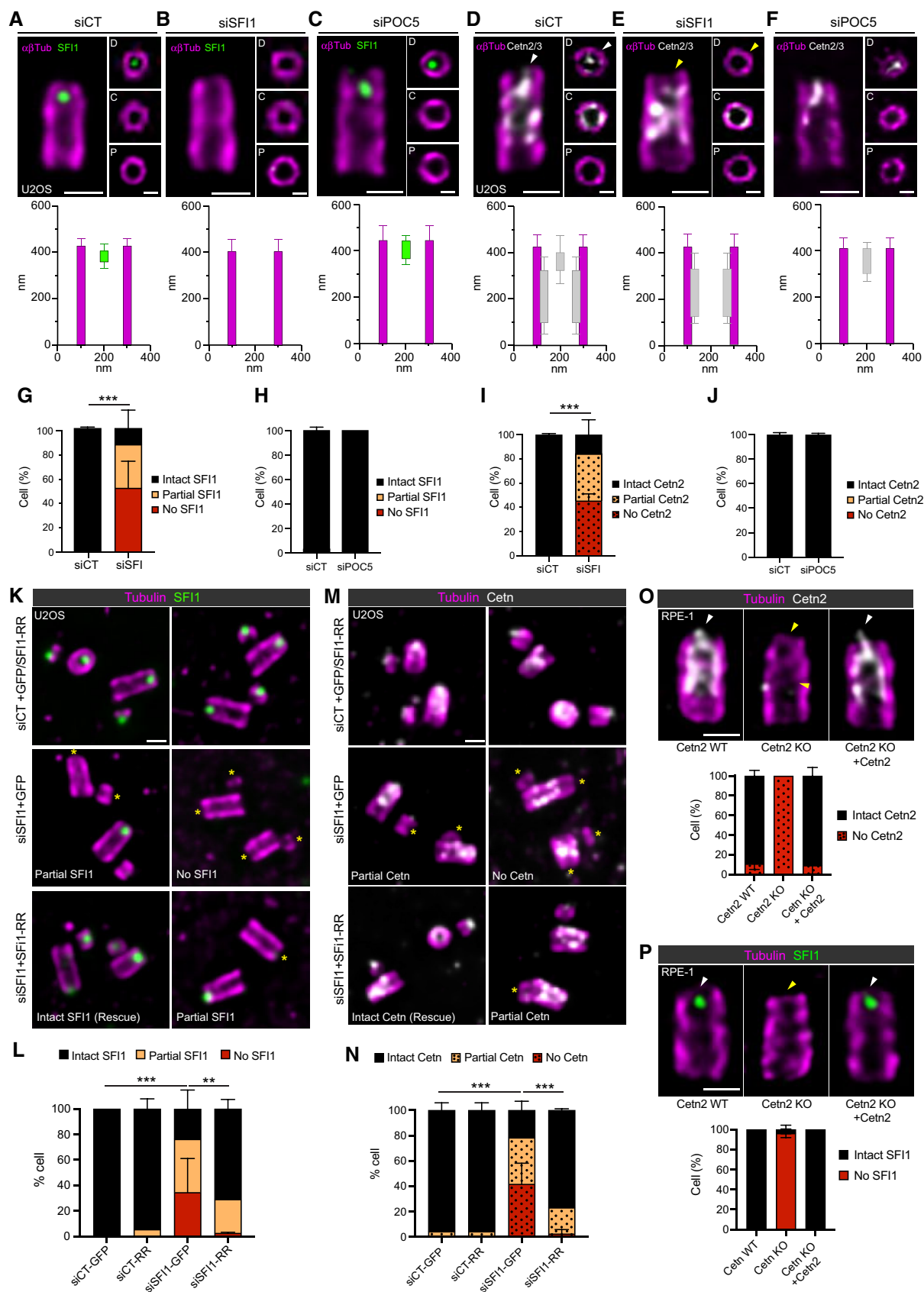
Figure 3.

◀

Figure 3. SFI1 depletion prevents distal Centrin recruitment at centrioles.

A–F   Representative confocal images of expanded U2OS centrioles treated with siCT (A, D), siSFI1 (B, E), and siPOC5 (C, F) stained for α/β-tubulin (αβTub, magenta) and SFI1 (A–C, green) or Centrin 2/3 (D–F, gray). Insets show top views of expanded centrioles at different positions along the centriole (P = proximal, C = central, and D = distal). Note that in the absence of SFI1 and Centrin staining at the distal tip, the orientation of the centriole was decided based on the larger diameter of the proximal region compared to the distal one, as previously observed in cryo-tomography (Greenan *et al*, 2020). White arrowheads point to the distal dot of SFI1 and Centrin that disappear in SFI1-depleted (yellow arrowheads) but not in POC5-depleted centrioles. Scale bars: 200 and 100 nm (inset). Longitudinal and radial localization of SFI1 and Centrin 2/3 in siCT (A, D), siSFI1 (B, E), and siPOC5 (C, F) are presented below the corresponding image.

G, H   Percentage of cells with centrioles SFI1-positive (intact SFI1), partially depleted (partial SFI1) or totally missing SFI1 (no SFI1) at the distal dot in siSFI1 (G) and siPOC5 (H) compared to control cells.

I, J   Percentage of centriole with a distal Centrin 2/3 signal in siSFI1 (I) and siPOC5 (J) compared to control cells.

K–N   Representative images of expanded U2OS cells expressing GFP alone or GFP + SFI1-RR and treated with siCT or siSFI1. Cells were stained for α/β-tubulin (αβTub, magenta) and SFI1 (K, green) or Centrin 2/3 (M, gray). A yellow asterisk indicates the centriole lacking SFI1 and Centrin distal dots. Scale bar: 250 nm. Expression of GFP + SFI1-RR in siSFI1 treated cell rescues the presence of SFI1 and Centrin at the distal tip of the centriole.

O, P   Representative confocal images of expanded Cetn2 WT, Cetn KO, or Cetn2 rescue RPE-1. Cells were stained for α/β-tubulin (αβTub, magenta) and Centrin 2 (O, gray) or SFI1 (P, green). Arrowheads indicate the presence (white) or the absence (yellow) of Centrin 2 and SFI1. Scale bar: 200 nm. Quantification shows the total absence of Centrin 2 in the KO cells correlating with the absence of SFI1. Both Centrin 2 and SFI1 localization are rescued when Centrin 2 is re-expressed in KO cells.

Data information: Average ± SD, *N*, statistical analysis: (A–F) *N* = 25, 40, 60, 29, 34 and 34 centrioles from three independent experiments. (G) siCT = Intact SFI1: 99.3% ± 0.9, Partial SFI1: 0.7% ± 1, No SFI1: 0% ± 0, siSFI1 = Intact SFI1: 13.1% ± 14.5, Partial SFI1: 35.1% ± 7.9, No SFI1: 51.8% ± 21.5. *N* = 3 independent experiments (> 80 centrioles per experiment). Two-way ANOVA (***P < 0.0001). (H) siCT = Intact SFI1: 97% ± 2.8, Partial SFI1: 3% ± 2.8, No SFI1: 0% ± 0, siSFI1 = Intact SFI1: 100% ± 0, Partial SFI1: 0% ± 0, No SFI1: 0% ± 0. *N* = 2 independent experiments (> 80 centrioles per experiment). Two-way ANOVA (P = 0.104) (I) siCT = Intact SFI1: 99.2% ± 1, Partial SFI1: 0.8% ± 1, No SFI1: 0% ± 0, siSFI1 = Intact SFI1: 15.6% ± 12.4, Partial SFI1: 39% ± 10.5, No SFI1: 45.4% ± 5.7. *N* = 3 independent experiments (> 80 centrioles per experiment). Two-way ANOVA (***P < 0.0001) (J) siCT = Intact SFI1: 99% ± 1.7, Partial SFI1: 1% ± 1.7, No SFI1: 0% ± 0, siSFI1 = Intact SFI1: 99.3% ± 1.15, Partial SFI1: 0.7% ± 1.15, No SFI1: 0% ± 0. *N* = 2 independent experiments (> 80 centrioles per experiment). Two-way ANOVA (P = 0.892). (L) siCT-GFP = Intact SFI1: 100% ± 0, Partial SFI1: 0% ± 0, No SFI1: 0% ± 0. siCT-RR = Intact SFI1: 94.4% ± 7.8, Partial SFI1: 5.6% ± 7.8, No SFI1: 0% ± 0. siSFI1-GFP = Intact SFI1: 24% ± 14.4, Partial SFI1: 41.6% ± 11.8, No SFI1: 34.6% ± 26.5. siSFI1-RR = Intact SFI1: 70.9% ± 7.4, Partial SFI1: 26.5% ± 6.7, No SFI1: 2.6% ± 0.6. *N* = 2 independent experiments (> 50 centrioles/experiments). Two-way ANOVA followed by Tukey's multiple comparison (siCT-GFP vs. siSFI1-GFP, ***P < 0.0001; siSFI1-GFP vs. siSFI1-RR, **P = 0.0032). (N) siCT-GFP = Intact Cetn: 95.8% ± 5.9, Partial Cetn: 4.2% ± 5.9, No Cetn: 0% ± 0. siCT-RR = Intact Cetn: 95.8% ± 5.9, Partial Cetn: 4.2% ± 5.9, No Cetn: 0% ± 0. siSFI1-GFP = Intact Cetn: 21.7% ± 7.1, Partial Cetn: 36.7% ± 9.4, No Cetn: 41.7% ± 16.5. siSFI1-RR = Intact Cetn: 77% ± 1.1, Partial Cetn: 20.6% ± 2.2, No Cetn: 2.4% ± 3.4. *N* = 2 independent experiments (> 50 centrioles/experiments). Two way ANOVA followed by Tukey's multiple comparison (siCT-GFP vs. siSFI1-GFP, ***P < 0.0001; siSFI1-GFP vs. siSFI1-RR, ***P < 0.0001). (O) Cetn2 WT = Intact Cetn2: 89.2% ± 5.7, No Cetn2: 10.8% ± 5.7; Cetn2 KO = Intact Cetn2: 0% ± 0, No Cetn2: 100% ± 0; Cetn2 KO + Cetn2 = Intact Cetn2: 90.9% ± 8.6, No Cetn2: 9.1% ± 8.6. Two-way ANOVA followed by Tukey's multiple comparison (Cetn2 WT vs. Cetn2 KO, P < 0.0001; Cetn2 KO vs. Cetn2 KO + Cetn2, P < 0.0001). (P) Cetn2 WT = Intact SFI1: 100% ± 0, No SFI1: 0% ± 0; Cetn2 KO = Intact SFI1: 3.8% ± 4.3, No SFI1: 96.2% ± 4.3; Cetn2 KO + Cetn2 = Intact SFI1: 100% ± 0, No SFI1: 0% ± 0. *N* = 3 independent experiment (> 20 centrioles/experiment). Two-way ANOVA followed by Tukey's multiple comparison (Cetn2 WT vs. Cetn2 KO, P < 0.0001; Cetn2 KO vs. Cetn2 KO + Cetn2, P < 0.0001).

discrepancy between the proposed duplication phenotype (Kodani *et al*, 2019) and our study, we analyzed SFI1 depletion using the previously reported siRNA (siRNA#B; Kodani *et al*, 2019) in both U2OS and HeLa cells (Fig EV3F–S). While we found that the depletion efficiency at the centriolar level was weaker with siRNA#B than with siRNA#A, we could nevertheless detect a significantly reduced level of SFI1 at centrioles both in HeLa (Fig EV3F, H and K) and U2OS (Fig EV3M, O and R) cells. Consistent with our data, we found that Centrin distal localization is reduced (Fig EV3G, L, N and S). However, we could not observe any difference in cells harboring procentrioles both in HeLa (47.5% in siCT vs. 57.1% in siSFI1) and U2OS (44.2% in siCT vs. 51.8% in siSFI1) (Fig EV3I and P). Collectively, these data demonstrate that SFI1 depletion does not affect centriole duplication in human cells, distinct from its role in SPB duplication.

SFI1 is required for centriole integrity

In our study, despite the absence of centriole duplication defects after SFI1 depletion, we nevertheless noticed that the architecture of mature centrioles appeared to be affected. Indeed, we observed that SFI1 depletion affects the canonical circular shape of the microtubule wall of mature centrioles without affecting centriolar diameter and length, even though we noted a wider distribution of sizes with shorter and longer centrioles (Fig 4F–H, Movie EV1). Furthermore, we found that 35, 39, and 21% of centrioles were structurally abnormal in SFI1-depleted U2OS, RPE-1, and HeLa cells, respectively (Figs 4I and J, 5H and EV3E), often with open, wider, or shorter microtubule walls (Fig EV4).

Since the SFI1/Centrin distal complex is recruited very early at the onset of centriole biogenesis, we next wondered whether the structural defects arose during procentriole assembly or later at the level of mature centrioles. To address this question, we imaged growing procentrioles seen in top view and quantified their "roundness index" and structural integrity. Interestingly, we observed no difference between control and SFI1-depleted procentrioles, suggesting that the observed structural defects do not arise during centriole assembly but rather reflect instability after centriole maturation (Fig 4K and L). Moreover, we noticed that the absence of microtubule wall observed in SFI1-depleted abnormal centrioles was correlated with the lack of the inner scaffold localization of Centrin (Fig 4M and N), while CP110 was still present at the tip of these centriolar microtubule wall structures (Fig EV4C and D). As our data showed that SFI1 depletion specifically leads to distal Centrin loss, it is likely that the absence of Centrin at the central core may be an indirect consequence of the microtubule wall defect. Finally, we ascertained that the structural defects observed upon SFI1 depletion were solely due to SFI1 loss, by expressing the untagged RNAi-resistant version of SFI1. We found that these defects were significantly rescued, with only 7% of cells displaying abnormal centrioles (Fig 4O and P), confirming that the observed structural defects are due to the depletion of SFI1.
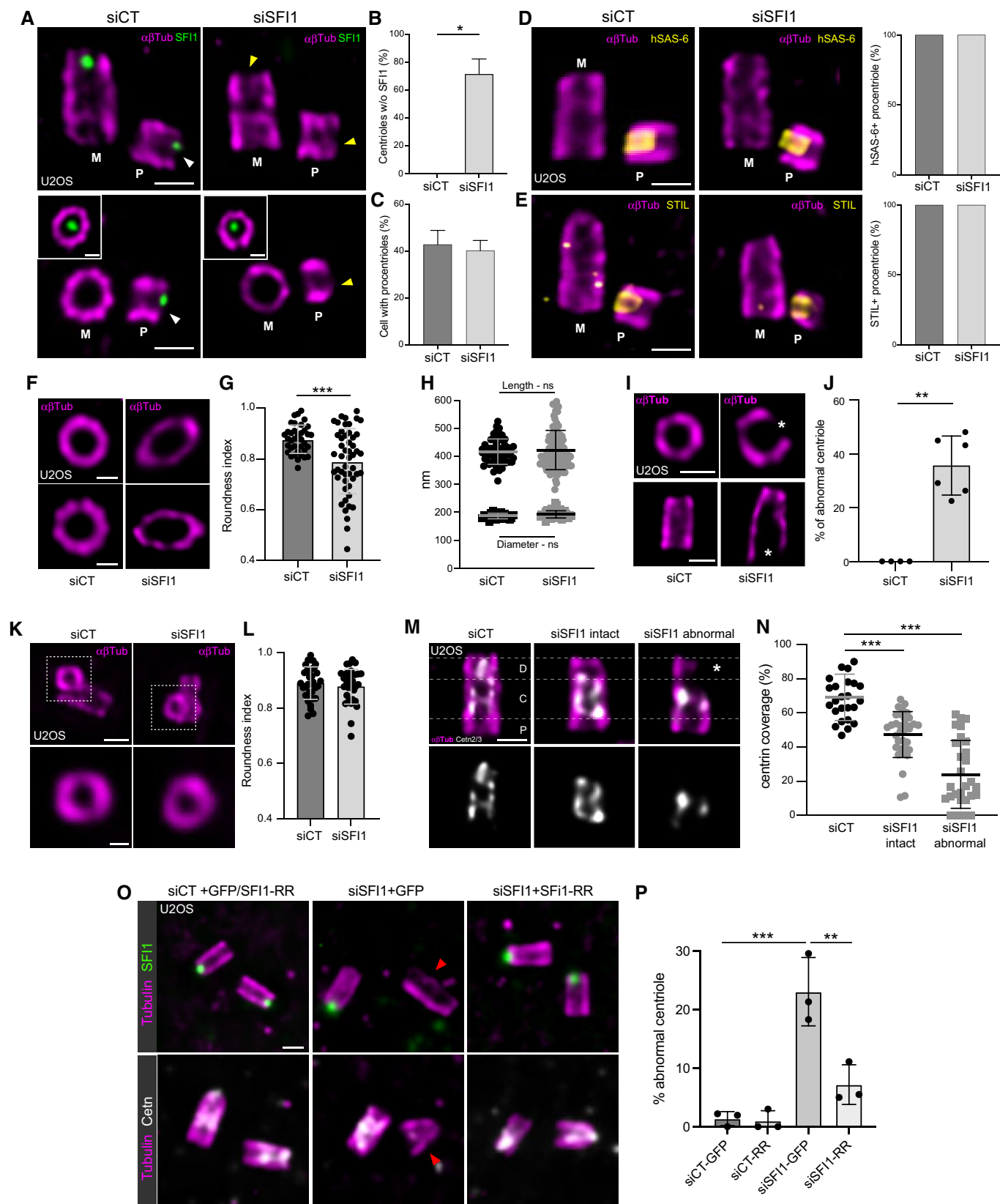
Figure 4.

◀

Figure 4. SFI1 is important for centriole architecture but not for duplication.

A Representative confocal images of expanded duplicating centrioles from siCT- and siSFI1-treated U2OS cells. Cells were stained for SFI1 (green) and α/β-tubulin (αβTub, magenta). The inset shows a distal position of the mother centriole where SFI1 signal is visible. The white arrowhead indicates the position of SFI1 distal dot in the procentriole of the control cell, which is lost in SFI1-depleted cells (yellow arrowhead). Scale bars: 200 nm.
B Quantification of the percentage of SFI1-negative procentrioles.
C Quantification of the percentage of duplicating centrioles.
D Representative confocal images of expanded duplicating centrioles from siCT and siSFI1 U2OS treated cells. Cells were stained for HsSAS-6 (yellow) and α/β-tubulin (αβTub, magenta). Quantification shows no difference in the percentage of HsSAS-6-positive centrioles in SFI1-depleted cells compared to control cells.
E Representative confocal images of expanded duplicating centrioles from siCT and siSFI1 U2OS treated cells. Cells were stained for STIL (yellow) and α/β-tubulin (αβTub, magenta). Quantification shows no difference in the percentage of STIL-positive centrioles in SFI1-depleted cells compared to control cells.
F Top views of expanded U2OS centrioles treated with siCT or siSFI1 stained for α/β-tubulin (αβTub, magenta). Scale bars: 200 nm.
G Roundness index of centrioles from siCT- and siSFI1-treated cells.
H Length (circle) and diameter (square) of expanded centrioles in siCT- or siSFI1-treated cells.
I Representative confocal images of expanded U2OS centrioles from siCT- and siSFI1-treated cells stained for α/β-tubulin (αβTub, magenta). White stars point to a broken microtubule wall. Scale bars: 200 nm.
J Percentage of abnormal centrioles in the indicated conditions.
K Top views of expanded procentrioles from U2OS cells treated with siCT or siSFI1 and stained for α/β-tubulin (αβTub, magenta). Scale bars: 200 nm.
L Roundness index of procentrioles from siCT- and siSFI1-treated cells.
M Representative confocal images of expanded U2OS centrioles from siCT- and siSFI1-treated cells stained for α/β-tubulin (αβTub, magenta) and Centrin (Cetn2/3, gray). White dashed lines delimitate the proximal, central, and distal regions. White star points to the broken microtubule wall. Scale bar: 200 nm.
N Centrin coverage (% of the total tubulin length) along the centriole in the indicated conditions.
O Representative images of expanded U2OS expressing GFP alone or GFP + SFI1-RR and treated with siCT or siSFI1. Cells were stained for α/β-tubulin (αβTub, magenta) and SFI1 (green) or Centrin 2/3 (gray). The red arrowhead indicates an abnormal centriole. Scale bar: 250 nm.
P Percentage of abnormal centrioles in the indicated conditions.

Data information: Average ± SD, *N*, statistical analysis: (B) siCT = 0% ± 0, siSFI1 = 71% ± 11. *N* = 4 independent experiment (50 centrioles per experiment), Mann–Whitney test (**P* = 0.028). (C) siCT = 43% ± 6, siSFI1 = 40% ± 4. *N* = 7 independent experiment (50 centrioles per experiment), Unpaired *t*-test (*P* = 0.3492). (D) siCT = 100% ± 0, siSFI1 = 100% ± 0. *N* = 3 independent experiments, Mann–Whitney test (*P* > 0.999). (E) siCT = 100% ± 0, siSFI1 = 100% ± 0. *N* = 3 independent experiments, Mann–Whitney test (*P* > 0.999). (G) siCT = 0.88 ± 0.05, siSFI1 = 0.79 ± 0.12. *N* = 37 and 50 for siCT and siSFI1 respectively from 4 independent experiments, Unpaired *t*-test (****P* = 0.0002). (H) siCT = 417 ± 45 nm (length) and 188 ± 10 nm (diameter), siSFI1 = 423 ± 71 nm (length) and 193.5 ± 13 nm (diameter). *N* = 50–90 for length and 30–40 for diameter from 4 independent experiments, Mann–Whitney test (*P* = 0.8440 (length), *P* = 0.079 (diameter)). (J) siCT = 0% ± 0, siSFI1 = 35.7% ± 11. *N* = 4 and 6 independent experiments for siCT and siSFI1 respectively, Mann–Whitney test (***P* = 0.0095). (L) siCT = 0.89 ± 0.05, siSFI1 = 0.87 ± 0.06. *N* = 34 and 33 for siCT and siSFI1 respectively from 4 independent experiments, Unpaired *t*-test (*P* = 0.376). (N) siCT: 69% ± 13, siSFI1: 47% ± 13, siSFI1 abnormal: 24% ± 20. *N* = 25, 34, 29 centrioles for siCT, siSFI1, and siSFI1 abnormal respectively from two independent experiments. One-way ANOVA followed by Tukey's post-hoc test (siCT vs. siSFI ****P* < 0.0001, siCT vs. siSFI1 abnormal ****P* < 0.0001). (P) siCT-GFP: 1.4% ± 1.2, siCT-RR: 1% ± 1.7, siSFI1-GFP: 23.1% ± 5.8, siSFI1-RR: 7.2% ± 2. *N* = 3 independent experiments (> 50 centrioles/experiments). One-way ANOVA followed by Tukey's multiple comparison (siCT-GFP vs. siSFI1-GFP, ****P* = 0.0003; siSFI1-GFP vs. siSFI1-RR, ***P* = 0.0026).

SFI1/Centrin complex is important for ciliogenesis

Since Centrin is required for ciliogenesis (Delaval *et al*, 2011; Prosser & Morrison, 2015), we speculated that this function might be specifically related to the distal SFI1/Centrin complex, due to its close proximity to the transition zone for cilium formation. Therefore, we looked first at the presence of SFI1 and Centrin at the centriole during ciliogenesis. We found by immunofluorescence and U-ExM that SFI1 localizes and remains at the distal end of the ciliated centriole in RPE-1 cells (Fig 5A and B). Similarly, staining of Centrin in those cells revealed that the distal Centrin dot also remains in ciliated cells, indicating that the whole complex is retained in these conditions (Fig 5C, yellow arrowheads). Next, we investigated the impact of SFI1 depletion on ciliogenesis. As it was the case with Centrin depletion (Prosser & Morrison, 2015), we observed that only 26% of SFI1-depleted cells displayed a primary cilium stained with acetylated tubulin, in contrast to the 75% observed in control cells (Fig 5D and E). To further explore the roots of ciliogenesis defects, we then analyzed this phenotype using U-ExM, where we obtained a 91% depletion efficiency of SFI1 in RPE-1 cells (Fig 5F and G), with a reduction of ciliogenesis similar to our observation in regular immunofluorescence (Fig 5I and J). Interestingly, by investigating the distal centriolar protein CP110, which regulates ciliogenesis (Spektor *et al*, 2007), we found that 47% of the SFI1-depleted cells failed to remove CP110

from the centriole's distal end (Fig 5I and K), in contrast to the 90% of control cells that did so. This observation indicates that SFI1 participates in regulating CP110 removal, which could in part explain the observed ciliogenesis defects. Importantly, CP110 removal, as well as the ciliogenesis defect itself, could be rescued by re-expressing RNAi-resistant SFI1 (Fig 5L–N).

These results are consistent with the previously described function of Centrin 2 in regulating CP110 removal during ciliogenesis (Prosser & Morrison, 2015), reinforcing our hypothesis that this process occurs through the SFI1/Centrin complex. Therefore, we then assessed whether the distribution pattern of the distal appendage protein CEP164 was also affected, as already reported by regular immunofluorescence in Centrin 2 knock-out cells (Prosser & Morrison, 2015). Remarkably, we found by U-ExM that, while we could clearly observe the 9-fold distribution of CEP164 around the mature centriole in control cells, this organization was markedly affected in SFI1-depleted ciliated and cycling RPE-1 cells (Fig 6A–D, I and K). We then explored whether the structural defects observed upon SFI1 depletion could be correlated to the disrupted CEP164 distribution pattern. However, we found no correlation between these two defects, showing that CEP164 loss is not directly due to structural abnormalities but rather directly related to the depletion of SFI1 (Fig EV5). We next sought an alternative explanation and tested whether appendage anchoring on triplet microtubules might be affected. To do so, we stained for the protein CEP90, which has
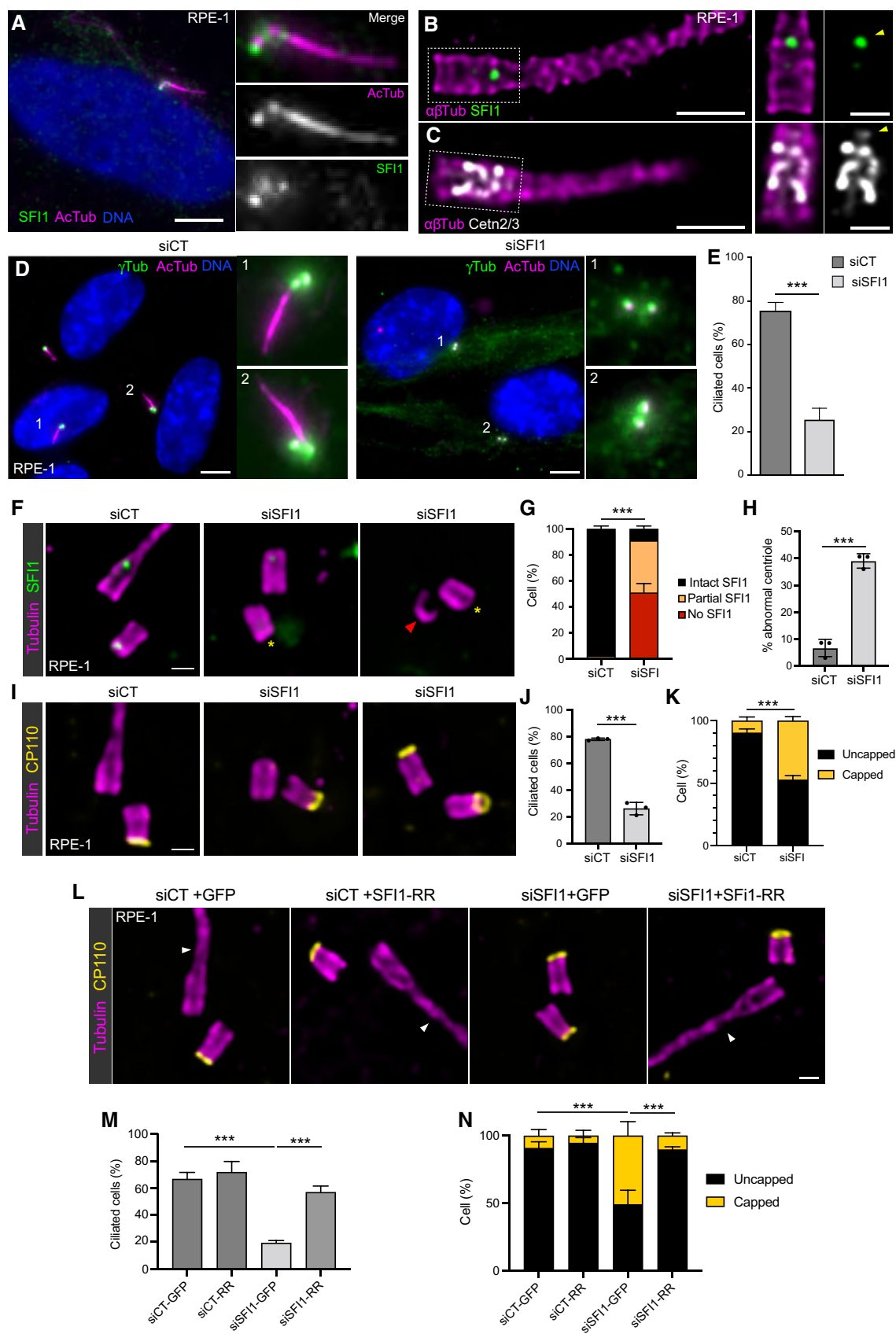
Figure 5.

Figure 5. SFI1 controls CP110 removal and ciliogenesis.

A   Representative confocal images of serum-starved RPE-1 cells stained for SFI1 (green) and acetylated tubulin (AcTub, magenta). Scale bar: 5 μm.

B, C Representative confocal images of serum-starved expanded RPE-1 stained for SFI1 (B, green) or Centrins (C, Cetn2/3, gray) and α/β-tubulin (αβTub, magenta). Insets show single channels depicting the distal localization of SFI1 (B, arrowhead) and Centrins (C, arrowhead). Scale bars: 500 and 200 nm (inset).

D   Representative confocal images of serum-starved RPE-1 cells transfected with control or SFI1 siRNA stained for γ-tubulin (γTub, green) and acetylated tubulin (AcTub, magenta) and DNA (DAPI, blue). Scale bar: 5 μm.

E   Percentage of ciliated cells in the indicated conditions.

F   Representative widefield images of expanded centrioles during ciliogenesis from siCT and siSFI1 RPE-1 treated cells. Cells were stained for α/β-tubulin (magenta) and SFI1 (green). Yellow asterisks indicate the absence of SFI1 at the distal tip of the centrioles. The red arrowhead indicates an abnormal centriole. Scale bar: 250 nm.

G   Percentage of RPE-1 cells with centrioles SFI1-positive (intact SFI1), partially depleted (partial SFI1) or totally missing SFI1 (no SFI1) at the distal dot in siSFI-treated cells.

H   Percentage of abnormal centrioles in RPE-1 cells treated with siSFI1.

I   Representative widefield images of expanded centrioles during ciliogenesis from siCT and siSFI1 RPE-1 treated cells. Cells were stained for α/β-tubulin (magenta) and CP110 (yellow). Scale bar: 250 nm.

J   Percentage of ciliated cells observed in U-ExM under the indicated conditions.

K   Percentage of CP110 capped/uncapped centrioles under the indicated conditions.

L   Representative widefield images of expanded RPE-1 during ciliogenesis, expressing GFP alone or GFP + SFI1-RR and treated with siCT or siSFI1. Cells were stained for α/β-tubulin (αβTub, magenta) and CP110 (yellow). Arrowheads indicate a cilium. Scale bar: 250 nm.

M   Percentage of ciliated cells observed in U-ExM in the indicated conditions.

N   Percentage of CP110 capped/uncapped centrioles in the indicated conditions.

Data information: Average ± SD, N, statistical analysis: (E) siCT = 75% ± 3, siSFI1 = 26% ± 6. N = 3 independent experiments (100 cells per experiment), unpaired *t*-test (***P = 0.0002). (G) siCT = Intact SFI1: 97.8% ± 2.3, Partial SFI1: 2.2% ± 2.3, No SFI1: 0% ± 0, siSFI1 = Intact SFI1: 9.1% ± 2.3, Partial SFI1: 40% ± 4.8, No SFI1: 51.6% ± 7.9. N = 3 independent experiments (> 50 centrioles per experiment). Two-way ANOVA (***P < 0.0001). (H) siCT: 6.6% ± 3.2, siSFI1: 39.1% ± 2.7. N = 3 independent experiments (> 50 centrioles/experiment). Welch's test (***P = 0.002). (J) siCT: 77.9% ± 0.9, siSFI1: 26.3% ± 4.6. N = 3 independent experiments (> 50 centrioles/experiment). Unpaired *t*-test (***P < 0.0001). (K) Uncapped = siCT: 90.4% ± 3.1, siSFI1: 52.6% ± 3.4; Capped = siCT: 9.6% ± 3.1, siSFI1: 47.4% ± 3.4. N = 3 independent experiments (> 50 centrioles/experiment). Two-way ANOVA (***P < 0.0001). (M) siCT-GFP: 66.7% ± 5, siCT-RR: 71.8% ± 7.9, siSFI-GFP: 19.4% ± 1.7, siSFI1-RR: 57% ± 4.6. N = 3 independent experiments (> 50 centrioles/experiments). One-way ANOVA followed by Tukey's multiple comparison (siCT-GFP vs. siSFI-GFP ***P < 0.0001, siSFI-GFP vs. siSFI1-RR ***P = 0.0001). (N) Uncapped = siCT-GFP: 90.9% ± 4.7, siCT-RR: 94.6% ± 4, siSFI-GFP: 49.1% ± 10.5, siSFI-RR: 89.8% ± 2.1. Capped = siCT-GFP: 9.1% ± 4.7, siCT-RR: 5.4.6% ± 4, siSFI-GFP: 50.9% ± 10.5, siSFI-RR: 10.2% ± 2.1. N = 3 independent experiments (> 50 centrioles/experiments). Two-way ANOVA (***P < 0.0001).

been recently proposed to be at the base of appendages (Kumar *et al*, 2021; Le Borgne *et al*, 2022). We did not observe any major defect of CEP90 localization (Fig 6E–H, J and K), suggesting that CEP164 defects may be due to an as-yet undescribed direct regulatory mechanism between the SFI1 protein and CEP164.

Overall, our results demonstrate that SFI1 is a centriolar protein that forms a complex with Centrin at the earliest stages of procentriole assembly. We also reveal that this complex is not required for centriole duplication, but rather is crucial for the maintenance of the correct centriolar architecture, such as the microtubule barrel and the organization of distal CEP164 appendages. Furthermore, we find that SFI1 is crucial for primary cilium formation, possibly because of its function in maintaining centriolar architecture, but also for its role in regulating CP110 removal (Fig 6L).

Discussion

The evolutionary origin of the centriole remains an enigma, but its near-ubiquitous existence in eukaryotes, as well as phylogenetic analyses, have led to propose that this organelle was already present in the Last Eukaryotic Common Ancestor (Azimzadeh & Marshall, 2010; Carvalho-Santos *et al*, 2010; Hodges *et al*, 2010; Azimzadeh, 2014, 2021). Over millions of years of evolution, the molecular architecture of the centriole has been preserved in parts in many species but disappeared in some cases concomitantly with the loss of a motile flagellum (Azimzadeh & Marshall, 2010), such as in yeasts, amoebozoa and flowering plants (Nabais *et al*, 2020). Nevertheless, yeasts retain a rudimentary organelle, the SPB, which

shows some similarities with the centriole, such as duplication and assembly processes that are tightly linked to the cell cycle (Seybold & Schiebel, 2013).

In yeast, SPB duplication is characterized by the formation of a half-bridge structure, made of Cdc31 and Sfi1, that provides a structural platform for SPB duplication (Spang *et al*, 1995; Jaspersen *et al*, 2002; Kilmartin, 2003; Bouhlel *et al*, 2015). Intriguingly, SFI1 and Centrins are also present in mammalian centrosomes, but whether they form a complex at centrioles and are involved in centriole duplication remained unclear. In this paper, we establish that SFI1 is a *bona fide* centriolar protein that is recruited early during centriole biogenesis at its growing distal end. Importantly, we found that a pool of Centrin displays a similar localization at the distal end of centrioles in addition to the previously described inner scaffold localization (Le Guennec *et al*, 2020; Steib *et al*, 2020). In addition, we noticed that the Centrin 3 signal is slightly less extended (Fig 1G and H) but this difference might be due to either the quality of the antibody or to a real difference between the two Centrins. By measuring at nanometric scale precision the distance between the Centrin and SFI1 signals, we found that these proteins are about 35 nm distant from each other, which is negligible if we consider that the size of 15 SFI1 repeats is about 60 nm long (Li *et al*, 2006) and that the SFI1 antibody recognizes its C-terminus and not the repeats region. Moreover, biophysical data showed that these proteins interact directly *in vitro* (Martinez-Sanz *et al*, 2006, 2010). Taken together, we can assert that the SFI1/Centrin complex is conserved in mammals and that it is localized at the distal end of centrioles, from the early stages of procentriole assembly.
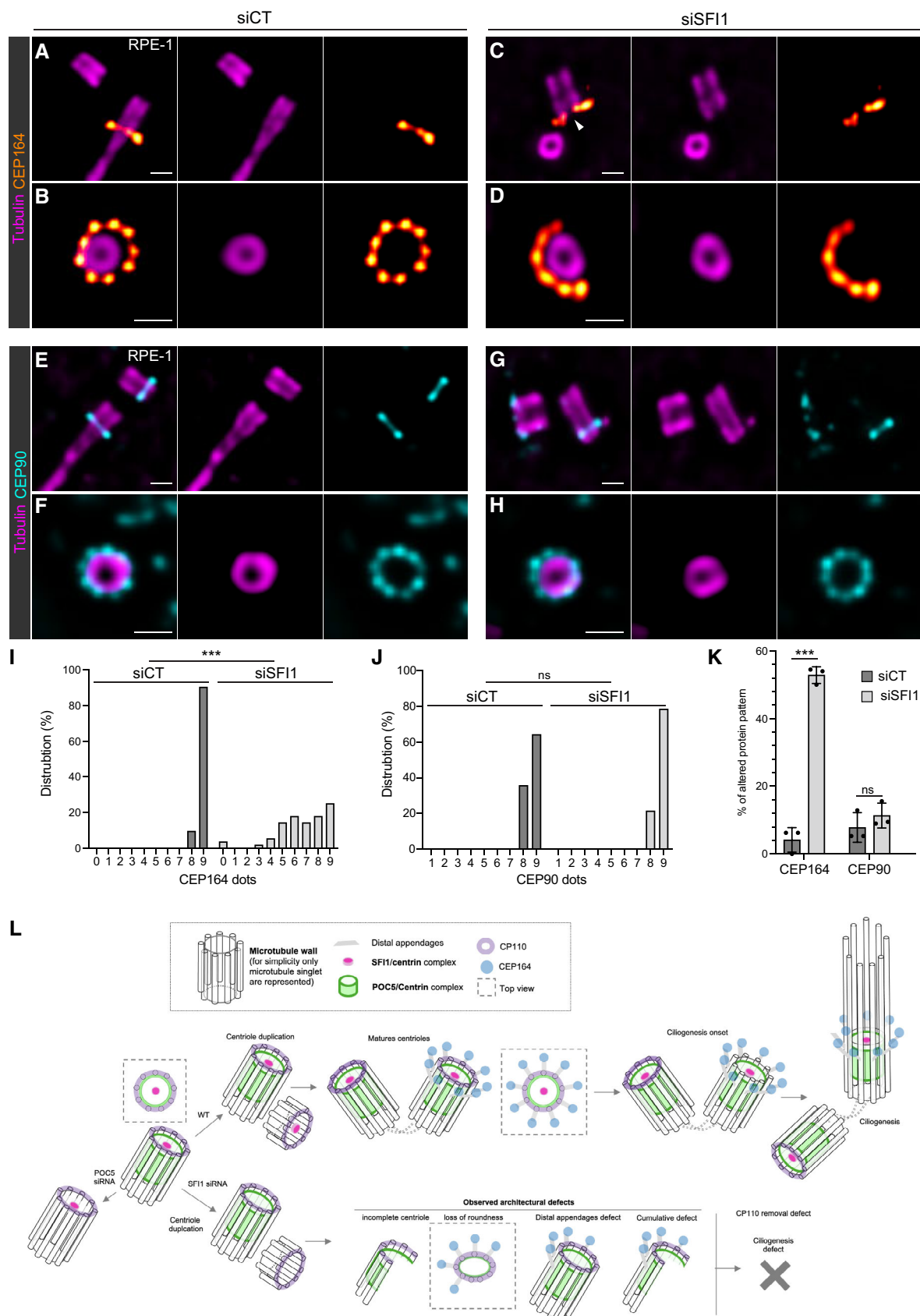
Figure 6.

Figure 6. SFI1 depletion impacts the distal appendage CEP164 protein organization.

A–D   Representative widefield images of expanded centrioles during ciliogenesis from siCT (A, B) and siSFI1 (C, D) RPE-1 treated cells. Cells were stained for α/β-tubulin (magenta) and CEP164 (red hot). Note the abnormal organization of the distal appendage protein CEP164 in siSFI1-treated cells. Scale bar: 250 nm.

E–H   Representative widefield images of expanded centrioles during ciliogenesis from siCT (E, F) and siSFI1 (G, H) RPE-1 treated cells. Cells were stained for α/β-tubulin (magenta) and CEP90 (cyan). Scale bar: 250 nm.

I   Frequency distribution of the number of dots per centriole formed by CEP164 in the indicated conditions.

J   Frequency distribution of the number of dots per centriole formed by CEP90 in the indicated conditions.

K   Percentage of cells presenting abnormal CEP164 and CEP90 in the indicated conditions.

L   Model of SFI1/Centrin localization and function at the distal end of human centrioles.

Data information: Average ± SD, N, statistical analysis: (I) siCT = 0–7 dots: 0%, 8 dots: 9.5%, 9 dots: 90.5%. siSFI1 = 0 dot: 3.6%, 1–2 dots: 0%, 3 dots: 1.8%, 4 dots: 5.4%, 5 dots: 14.3%, 6 dots: 17.9%, 7 dots: 14.3%, 8 dots: 17.9%, 9 dots: 25. $N = 21$ and 56 centrioles for siCT and siSFI1 respectively from three independent experiments. Mann–Whitney test (***$P < 0.0001$). (J) siCT = 0–7 dots: 0%, 8 dots: 35.7%, 9 dots: 64.3%. siSFI1 = 0–7 dots: 0%, 8 dots: 21.4%, 9 dots: 78.6%. $N = 14$ and 28 centrioles for siCT and siSFI1 respectively from three independent experiments. Mann–Whitney test ($P = 0.459$). (K) siCT = CEP164: 4.2% ± 3.6, CEP90: 7.8% ± 4.4. siSFI1 = CEP164: 52.8% ± 2.5, CEP90: 11.4% ± 3.7. $N = 3$ independent experiments (> 50 centrioles/experiments). Two-way ANOVA followed by Sidak's multiple comparison (CEP164 siCT vs. siSFI1, ***$P < 0.0001$; CEP90 siCT vs. siSFI1, $P = 0.607$).

Additionally, we demonstrated that SFI1 is critical for Centrin targeting at the distal end of centrioles. On the other hand, we established that POC5 drives the localization of Centrin at the inner scaffold region of centrioles while it does not affect the distal pool of Centrin or SFI1. Altogether, these results highlight the presence of two distinct complexes containing Centrin: one at the distal end of the centriole dependent on SFI1 and one at the central core relying on POC5.

In SFI1-depleted cells, we observed a decrease in Centrin signal that is consistent with the reduced GFP-Centrin 1 levels seen in a screen for centriole biogenesis factors (Balestra *et al*, 2013) as well as the reduced Centrin seen in a previous knockdown study (Kodani *et al*, 2019) that most likely led to the hypothesis that SFI1 depletion impairs centriole duplication. However, by directly monitoring pro-centriole formation using U-ExM, we demonstrated that centriole duplication is not affected in SFI1-depleted U2OS and HeLa cells. These observations indicate that the SFI1/Centrin complex is present at centrioles but does not participate in the initiation of centriole duplication in humans, unlike its yeast counterpart. Instead, SFI1 depletion leads to structurally abnormal centrioles, which lose their canonical organization. In addition, we also revealed that SFI1 is important for ciliogenesis and that this defect derives from defective CP110 uncapping and altered CEP164 distribution. This phenotype is fully consistent with the reported Centrin 2 knockout defects (Prosser & Morrison, 2015), emphasizing that SFI1 and Centrin might act as a complex also in humans. Intriguingly, we did not observe structurally abnormal centrioles in the RPE1 Centrin 2 knockout cells. However, we found that while Centrin 2 was absent from centrioles, staining of Centrin 3 in these cells revealed that it clearly remained at the level of the central core (Appendix Fig S3). Therefore, we hypothesize that Centrin 3 could compensate for the loss of Centrin 2 only at the inner scaffold level, thus preventing structural defects and maintaining the overall stability of mature centrioles.

Another intriguing question concerns the molecular organization of SFI1/Centrins inside centrioles. In yeast, Sfi1 molecules form two anti-parallel arrays connected by Sfi1 C-termini, with the N-termini oriented towards the SPB cores (Li *et al*, 2006). In our study, we focused on localizing the C-terminus of human SFI1. If the C-terminal interactions are conserved in spite of strong sequence divergence between yeast and human SFI1 outside the Centrin-binding domains, we can imagine that SFI1 C-termini could interact in the center of the centriolar lumen, while the N-terminal domains radially extend towards the periphery, facing the centriolar microtubule walls at the distal end, similar to the cartwheel structure found in the proximal region. However, this remains difficult to probe now owing to the lack of appropriate tools. Such a radial structure has never been observed in the centriole, but it is likely that another type of assembly exists there. Indeed a recent study has shown that C2CD3 and LRRCC1 also localize at the lumenal distal end of the human centriole (Gaudin *et al*, 2022), similarly to SFI1 and Centrin, and delineate a structure reminiscent of the acorn, a filamentous density observed by electron microscopy in pro and mature *Chlamydomonas* basal bodies (Geimer, 2004; Gaudin *et al*, 2022). In addition, the acorn is accompanied by a V-shaped filament system that has been proposed to be composed of Centrin (Geimer & Melkonian, 2005). It is therefore possible that SFI1 and Centrin are part of this V-shaped filament system and associate with other distal extremity centriolar proteins, such as C2CD3 and LRRCC1, to ensure proper centriole formation and stability.

It will also be necessary to better understand the function of the different Centrins in humans and whether they form separate complexes with SFI1 or co-assemble in the same ones if co-expressed in the same cell. Since Centrin 1 is only expressed in the testis and Centrin 4 in ciliated cells and in the retina, they might assume cilia−/flagella-specific functions, while Centrin 2 or Centrin 3 could be mainly involved in centriole functions. Solving these questions would certainly help fully understand the function of the SFI1/Centrin complex in human centrioles.

Materials and Methods

Human cell lines and cell culture

RPE-1 (ATCC) and RPE-1 Cent2 KO cells (Prosser & Morrison, 2015) were cultured in DMEM medium supplemented with 10% fetal calf serum and 1% penicillin–streptomycin at 37°C and 5% CO_2. To induce ciliogenesis, cells were starved from serum for 48 h (DMEM + 0.5% FCS). U2OS (ATCC) and HeLa (gift from I. Gasic lab) cells were cultured in DMEM supplemented with GlutaMAX (Life Technology), 10% tetracycline-negative fetal calf serum (life technology), penicillin, and streptomycin (100 μg/ml) at 37°C and 5% CO_2. Cells were tested for mycoplasma contaminations regularly.

Cloning

The following plasmid was used in the study: SFI1-GFP (Kilmartin, 2003), SFI1-SNAP (Lukinavičius *et al*, 2013), and SFI1-mcherry (Gift from J. Azimzadeh).

For the rescue experiment, an RNAi-resistant version of SFI1 was obtained by directed mutagenesis using QuikChange II Site-Directed Mutagenesis Kit (Agilent) such as position (816–837 bp) 5′-AAGGTTGTC TCTGCAGTGAAA-3′ which correspond to siRNA#A was modified for 5′-AAAGTCGTGAGTGCTGTCAAG-3′. SFI1-RR gene was PCR amplified allowing the insertion of BglII upstream of the start codon. PCR-amplified SFI1-RR was subcloned into the pIRES-GFP vector BglII-digested and dephosphorylated. Positive clones were sequenced and amplified.

SFI1 depletion using siRNAs and rescue experiment

Three siRNAs were used to deplete SFI1. siSFI1#A and siSFI1#A′ were designed as described in (Balestra *et al*, 2013); siSFI1#B were designed as described in (Kodani *et al*, 2019), and purchased from Eurogentec. The sequences are as follows:

siSFI1#A (AAGCAAGTACTCATTACAGAA-dTdT)
siSFI1#A′ (AAGGTTGTCTCTGCAGTGAAA-dTdT)
siSFI1#B (CAACAAGAAGUCUUCUGCAUCCUUU)

The silencer select negative control siRNA1 used as siControl#A was purchased from Thermo Fisher (4390843, Thermo Fisher). The ON-TARGET plus Non-targeting Pool siRNA used as negative control siControl#B was purchased from Dharmacon (Catalog #D-001810-10-20). Cells were plated at 100,000 cell/well (RPE-1 and HeLa) or 150,000 cells /well (U2OS) on 12 mm coverslips in a 6-well plate for 24 h and transfected with siRNA using lipofectamine RNAi MAX reagents (Invitrogen) according to the manufacturers' protocol. We either used 10 nM for siControl#A (siCT#A), siSFI1#A and siSFI1#A′ or 50 nM for siCT#B and siSFI1#B. The medium was changed 5 h post-transfection and cells were analyzed 72 h after transfection.

For the rescue experiment, cells were seeded as described for 24 h and transfected with 2.5 μg of pIRES-GFP or pIRES-GFP-SFI1-RR using 5 μl of JetPrime per well, according to the manufacturers' instructions. The medium was changed 5 h post-transfection and control#A or SFI1 siRNA was transfected into the cell as described above. The medium was changed 5 h post-transfection and cells were analyzed 72 h after transfection.

POC5 depletion using siRNAs

U2OS cells were plated at 100,000 cell/well on 12 mm coverslips in a 6-well plate for 24 h and transfected with 25 nM of silencer select negative control siRNA1 (4390843, Thermo Fisher) or siPOC5 (siPOC5: 5′-CAACAAAUUCUAGUCAUACUU-3′) (Azimzadeh *et al*, 2009) using Lipofectamine RNAi MAX reagents (Invitrogen) according to the manufacturers' protocol. The medium was changed 6 h post-transfection and cells were analyzed 72 h after transfection.

Antibodies

The SFI1 antibody was raised in rabbits against a GST-fused C-terminal domain of SFI1 (aa1021 to aa1240) (Appendix Fig S1) and

affinity-purified on AminoLink® Coupling Resin (20381 Thermo Fisher) coupled to the MBP-fused C-terminal domain (using the same target peptide sequence).

Antibodies used in this stud: SFI1 (13550-1-AP, Proteintech Europe, 1:1,000 for IF and 1:250 for U-ExM), home-made SFI1 (this study, 1:200), γ-tubulin (sc-7396, Santa Cruz Biotechnology, Inc., 1:500), Centrin (clone 20H5, 04-1624, Millipore, 1:500 for IF and 1:250 for U-ExM), Centrin 2 (15877-1-AP, Proteintech, 1:1,000), Centrin 3 (H00001070-M01, Abnova, 1:250), PCNA (mAb #2586, Cell Signalling Technology, 1:1,000), HsSAS-6 (sc-81431, sc-98506 Santa Cruz Biotechnology, Inc. 1:250), STIL (A302-441A-T, Bethyl, 1:250), CP110 (EPP11816, Elabscience, 1:1,000 for IF and 1:500 for U-ExM), CEP164 (2227-1-AP, Proteintech, 1:500), CEP90 (144-1-AP, Proteintech, 1:250), acetylated tubulin (Institut Curie Recombinant antibodies Platform, 1:75), β-tubulin (AA344, scFv-S11B, 1:250), and α-tubulin (AA345, scFv-F2C, 1:250) (Nizak *et al*, 2003), α-tubulin (ab18251, Abcam, 1:500) and anti-tubulin YL1/2 (ab6160, Abcam, 1:250) were purchased from the indicated suppliers. Secondary fluorescent antibodies were purchased from Invitrogen (A11008, A11004, A11029, and A11036, Invitrogen, ThermoFisher) and used at 1:800 dilutions for standard immunofluorescence experiments and 1:400 for U-ExM.

Immunofluorescence microscopy

For immunofluorescence microscopy, cells were grown on 12 mm coverslips and fixed at −20°C with cold methanol for 3 min. Fixed cells were then incubated with the primary antibodies for 1 h at room temperature, washed with PBS, and subsequently incubated with the secondary antibodies conjugated with Alexa Fluor-488, 594, or 647. DNA was counterstained with DAPI solution. Samples were mounted in Mowiol and observed with a fluorescence microscope (Upright Leica DMI-5000B) equipped with a CCD Camera 1,392 × 1,040 (CoolSnap HQ2 pixel: 6.45 μm from Photometrics). Images were acquired and processed using Metamorph software (Molecular Devices). For the quantification of fluorescence intensity (Fig 3B), maximal projections were analyzed using Fiji (Schindelin *et al*, 2012). Confocal centriolar intensities were assessed by individual plot profiles along a linescan of 30 pixels on each pair of mature centrioles. For each experiment, all values were normalized on the average value of the control cells to obtain the relative intensity (A.U.). An average of all normalized measures was generated and plotted in GraphPad Prism7.

Ultrastructure expansion microscopy (U-ExM)

The following reagents were used in U-ExM experiments: formaldehyde (FA, 36.5–38%, F8775, SIGMA), acrylamide (AA, 40%, A4058, SIGMA), N, N′-methylenbisacrylamide (BIS, 2%, M1533, SIGMA), sodium acrylate (SA, 97–99%, 408220, SIGMA and 7446-81-3, AK Scientific), ammonium persulfate (APS, 17874, ThermoFisher), tetramethylethylendiamine (TEMED, 17919, ThermoFisher), nuclease-free water (AM9937, Ambion-ThermoFisher), and poly-D-lysine (A3890401, Gibco).

RPE-1, U2OS, and HeLa cells were grown on 12 mm coverslips and processed for expansion as previously described (Le Guennec *et al*, 2020; Steib *et al*, 2020). Briefly, coverslips were incubated in 2% AA + 1.4% FA diluted in PBS for 3–5 h at 37°C prior to gelation in monomer solution (19% sodium acrylate, 0.1% bis-

acrylamide, and 10% acrylamide) supplemented with TEMED and APS (final concentration of 0.5%) for 1 h at 37°C. Denaturation was performed for 1 h 30 min at 95°C and gels were stained as described above. For each gel, a caliper was used to accurately measure its expanded size. The gel expansion factor was obtained by dividing the size after expansion by 12 mm, which corresponds to the size of the coverslips use for sample seeding. Measurements of lengths and diameters were scaled according to the expansion factor of each gel.

Image acquisition and analysis

Expanded gels were mounted onto 24 mm coverslips coated with poly-D-lysine (0.1 mg/ml) and imaged with either an inverted wide-field Leica DM18 microscope or a confocal Leica TCS SP8 microscope. For the widefield imaging, images were taken with a 63× 1.4 NA oil immersion objective using the Thunder "Small volume computational clearing" mode and water as "Mounting medium" to generate deconvolved images. 3D stacks were acquired with 0.21 μm z-intervals and a 100 nm x, y pixel size. For the confocal imaging, images were taken with a 63× 1.4 NA oil objective with lightning mode at max resolution, adaptive as "Strategy" and water as "Mounting medium" to generate deconvolved images. 3D stacks were acquired with 0.12 μm z-intervals and a 35 nm x, y pixel size. Length, diameter, protein coverage, and relative protein position quantifications were performed as previously published in (Le Guennec *et al*, 2020). To generate the panels in Figs 1D, F, H and J and 3D–F, we used two homemade plugins for ImageJ as described previously (Le Borgne *et al*, 2022).

For the measurement of SFI1 intensity from regular IF (Figs EV1E and EV2), the Fiji plot profile tool was used to obtain the fluorescence intensity profile from proximal to distal for tubulin and SFI1 from the same line scan. For the measurement of SFI1 intensity from U-ExM (Fig EV3K, L, R and S), a 20 × 20 pixel square was positioned around the centrosome or in the vicinity to evaluate the background and mean intensity was measured in both regions. Background value was subtracted and data were plotted as mean intensity values for SFI1 and Centrin.

Measurement of centriolar roundness was performed on perfectly imaged top views of mature centrioles (Fig 4G) or procentrioles (Fig 4L) using the free shape tool to follow the tubulin signal. The roundness index was calculated using Fiji.

siRNA efficiency was evaluated manually at the level of the centriole from cells in either G1 (two centrioles) or S/G2 (four centrioles) phase (Figs 3G, I and L–P, 4B, 5G, EV1Q and R and EV3A, B, H and O). The intensity was increased to maximum (see Fig EV1L and M) and the signal was monitored. Data were classified into three categories: intact signal when all the centrioles were positive for the protein of interest, partial signal when one to three of the centrioles were lacking the protein signal, and no signal when the protein of interest was absent from all the centrioles.

For the quantification of the distal appendage organization, the number of CEP164 or CEP90 dots was manually quantified per centriole and reported as frequency distribution (%).

Statistical analysis

The comparison of the two groups was performed using an unpaired two-sided Student's *t*-test or its non-parametric correspondent, the Mann–Whitney test, if normality was not granted because rejected by the Pearson test. The comparisons of more than two groups were made using one-way ANOVAs followed by *post hoc* tests as indicated in the corresponding figure legend to identify all the significant group differences. *N* indicates independent biological replicates from distinct samples. Every experiment was performed at least three times independently on different biological samples unless specified. No statistical method was used to estimate the sample size. No blinding was applied for the analysis of the data. Data are all represented as scatter dot plots with the centerline as mean, except for percentage quantifications, which are represented as histogram bars. The graphs with error bars indicate SD ($\pm$) and the significance level is denoted as usual (*$P < 0.05$, **$P < 0.01$, ***$P < 0.001$, ****$P < 0.0001$). All the statistical analyses were performed using Excel or Prism7 (Graphpad version 7.0a, April 2, 2016).

Data availability

This study includes no data deposited in external repositories. Further information and requests for resources and reagents should be directed to Anne Paoletti (anne.paoletti@curie.fr), Paul Guichard (paul.guichard@unige.ch), and Virginie Hamel (virginie.hamel@unige.ch).

Expanded View for this article is available online.

Author contributions

Marine H Laporte: Data curation; formal analysis; validation; investigation; visualization; methodology; writing – original draft; writing – review and editing. **Imène B Bouhlel:** Data curation; formal analysis; investigation; visualization; methodology; writing – original draft. **Eloïse Bertiaux:** Data curation; formal analysis; visualization. **Ciaran G Morrison:** Data curation; formal analysis; validation; visualization; writing – review and editing. **Alexia Giroud:** Data curation; formal analysis. **Susanne Borgers:** Data curation; formal analysis; methodology. **Juliette Azimzadeh:** Methodology. **Michel Bornens:** Conceptualization. **Paul Guichard:** Conceptualization; supervision; funding acquisition; validation; writing – original draft; writing – review and editing. **Anne Paoletti:**

Conceptualization; supervision; funding acquisition; writing – original draft; writing – review and editing. **Virginie Hamel:** Conceptualization; supervision; validation; writing – original draft; writing – review and editing.

Disclosure and competing interests statement

The authors declare that they have no conflict of interest.

References

Azimzadeh J (2014) Exploring the evolutionary history of centrosomes. *Philos Trans R Soc Lond B Biol Sci* 369: 20130453

Azimzadeh J (2021) Evolution of the centrosome, from the periphery to the center. *Curr Opin Struct Biol* 66: 96–103

Azimzadeh J, Marshall WF (2010) Building the centriole. *Curr Biol* 20: R816–R825

Azimzadeh J, Hergert P, Delouvée A, Euteneuer U, Formstecher E, Khodjakov A, Bornens M (2009) hPOC5 is a centrin-binding protein required for assembly of full-length centrioles. *J Cell Biol* 185: 101–114

Balestra FR, Strnad P, Flückiger I, Gönczy P (2013) Discovering regulators of centriole biogenesis through siRNA-based functional genomics in human cells. *Dev Cell* 25: 555–571

Bauer M, Cubizolles F, Schmidt A, Nigg EA (2016) Quantitative analysis of human centrosome architecture by targeted proteomics and fluorescence imaging. *EMBO J* 35: 1–15

Baum P, Furlong C, Byers B (1986) Yeast gene required for spindle pole body duplication: homology of its product with Ca^{2+}–binding proteins. *Proc Natl Acad Sci USA* 83: 5512–5516

Bestul AJ, Yu Z, Unruh JR, Jaspersen SL (2017) Molecular model of fission yeast centrosome assembly determined by superresolution imaging. *J Cell Biol* 216: 2409–2424

Bornens M (2012) The centrosome in cells and organisms. *Science* 335: 422–426

Bouhlel IB, Ohta M, Mayeux A, Bordes N, Dingli F, Boulanger J, Velve Casquillas G, Loew D, Tran PT, Sato M *et al* (2015) Cell cycle control of spindle pole body duplication and splitting by Sfi1 and Cdc31 in fission yeast. *J Cell Sci* 128: 1481–1493

Boveri T (1900) *Ueber die Natur der Centrosomen. Zellen-Studien*, Vol. 4. Jena: Verlag von Gustav Fischer

Carvalho-Santos Z, Machado P, Branco P, Tavares-Cadete F, Rodrigues-Martins A, Pereira-Leal JB, Bettencourt-Dias M (2010) Stepwise evolution of the centriole-assembly pathway. *J Cell Sci* 123: 1414–1426

Carvalho-Santos Z, Azimzadeh J, Pereira-Leal JB, Bettencourt-Dias M (2011) Evolution: tracing the origins of centrioles, cilia, and flagella. *J Cell Biol* 194: 165–175

Dantas TJ, Wang Y, Lalor P, Dockery P, Morrison CG (2011) Defective nucleotide excision repair with normal centrosome structures and functions in the absence of all vertebrate centrins. *J Cell Biol* 193: 307–318

Delaval B, Covassin L, Lawson ND, Doxsey S (2011) Centrin depletion causes cyst formation and other ciliopathy-related phenotypes in zebrafish. *Cell Cycle* 10: 3964–3972

Gambarotto D, Zwettler FU, Le GM, Schmidt-cernohorska M, Fortun D, Borgers S, Heine J, Schloetel J, Reuss M, Unser M *et al* (2019) Imaging cellular ultrastructures using expansion microscopy (U-ExM). *Nat Methods* 16: 71–74

Gambarotto D, Hamel V, Guichard P (2021) Ultrastructure expansion microscopy (U-ExM). *Methods Cell Biol* 161: 57–81

Gaudin N, Martin Gil P, Boumendjel M, Ershov D, Pioche-Durieu C, Bouix M, Delobelle Q, Maniscalco L, Phan TBN, Heyer V *et al* (2022) Evolutionary conservation of centriole rotational asymmetry in the human centrosome. *Elife* 11: e72382

Gavet O, Alvarez C, Gaspar P, Bornens M (2003) Centrin4p, a novel mammalian centrin specifically expressed in ciliated cells. *Mol Biol Cell* 14: 1818–1834

Geimer S (2004) The ultrastructure of the *Chlamydomonas reinhardtii* basal apparatus: identification of an early marker of radial asymmetry inherent in the basal body. *J Cell Sci* 117: 2663–2674

Geimer S, Melkonian M (2005) Centrin Scaffold in *Chlamydomonas reinhardtii* revealed by immunoelectron microscopy. *Eukaryot Cell* 4: 1253–1263

Greenan GA, Vale RD, Agard DA (2020) Electron cryotomography of intact motile cilia defines the basal body to axoneme transition. *J Cell Biol* 219: e201907060

Hart PE, Glantz JN, Orth JD, Poynter GM, Salisbury JL (1999) Testis-specific murine centrin, Cetn1: genomic characterization and evidence for retroposition of a gene encoding a centrosome protein. *Genomics* 60: 111–120

Hinterndorfer K, Laporte MH, Mikus F, Petrozzi LT, Bourgoint C, Prouteau M, Dey G, Loewith R, Guichard P, Hamel V (2022) Ultrastructure expansion microscopy reveals the nanoscale cellular architecture of budding and fission yeast. *bioRxiv* https://doi.org/10.1101/2022.05.16.492060 [PREPRINT]

Hodges ME, Scheumann N, Wickstead B, Langdale JA, Gull K (2010) Reconstructing the evolutionary history of the centriole from protein components. *J Cell Sci* 123: 1407–1413

Ito D, Bettencourt-Dias M (2018) Centrosome remodelling in evolution. *Cell* 7: 71

Jaspersen SL, Giddings TH, Winey M (2002) Mps3p is a novel component of the yeast spindle pole body that interacts with the yeast centrin homologue Cdc31p. *J Cell Biol* 159: 945–956

Khouj EM, Prosser SL, Tada H, Chong WM, Liao J-C, Sugasawa K, Morrison CG (2019) Differential requirements for the EF-hands of human centrin2 in primary ciliogenesis and nucleotide excision repair. *J Cell Sci* 132: jcs228486

Kilmartin JV (2003) Sfi1p has conserved centrin-binding sites and an essential function in budding yeast spindle pole body duplication. *J Cell Biol* 162: 1211–1221

Kilmartin JV (2014) Lessons from yeast: the spindle pole body and the centrosome. *Philos Trans R Soc Lond B Biol Sci* 369: 20130456

Kodani A, Yu TW, Johnson JR, Jayaraman D, Johnson TL, Al-Gazali L, Sztriha L, Partlow JN, Kim H, Krup AL *et al* (2015) Centriolar satellites assemble centrosomal microcephaly proteins to recruit CDK2 and promote centriole duplication. *Elife* 4: 1–27

Kodani A, Moyer T, Chen A, Holland A, Walsh CA, Reiter JF (2019) SFI1 promotes centriole duplication by recruiting USP9X to stabilize the microcephaly protein STIL. *J Cell Biol* 218: 2185–2197

Kumar D, Rains A, Herranz-Pérez V, Lu Q, Shi X, Swaney DL, Stevenson E, Krogan NJ, Huang B, Westlake C *et al* (2021) A ciliopathy complex builds distal appendages to initiate ciliogenesis. *J Cell Biol* 220: e202011133

Laoukili J, Perret E, Middendorp S, Houcine O, Guennou C, Marano F, Bornens M, Tournier F (2000) Differential expression and cellular distribution of centrin isoforms during human ciliated cell differentiation *in vitro*. *J Cell Sci* 113: 1355–1364

Le Borgne P, Greibill L, Laporte MH, Lemullois M, Bouhouche K, Temagoult M, Rosnet O, Le Guennec M, Lignières L, Chevreux G *et al* (2022) The evolutionary conserved proteins CEP90, FOPNL, and OFD1 recruit

centriolar distal appendage proteins to initiate their assembly. *PLoS Biol* 20: e3001782

Le Guennec M, Klena N, Gambarotto D, Laporte MH, Tassin A, van den Hoek H, Erdmann PS, Schaffer M, Kovacik L, Borgers S *et al* (2020) A helical inner scaffold provides a structural basis for centriole cohesion. *Sci Adv* 6: eaaz4137

LeGuennec M, Klena N, Aeschlimann G, Hamel V, Guichard P (2021) Overview of the centriole architecture. *Curr Opin Struct Biol* 66: 58−65

Li S, Sandercock AM, Conduit P, Robinson CV, Williams RL, Kilmartin JV (2006) Structural role of Sfi1p–centrin filaments in budding yeast spindle pole body duplication. *J Cell Biol* 173: 867−877

Lukinavičius G, Lavogina D, Orpinell M, Umezawa K, Reymond L, Garin N, Gönczy P, Johnsson K (2013) Selective chemical crosslinking reveals a Cep57-Cep63-Cep152 centrosomal complex. *Curr Biol* 23: 265−270

Martinez-Sanz J, Yang A, Blouquit Y, Duchambon P, Assairi L, Craescu CT (2006) Binding of human centrin 2 to the centrosomal protein hSfi1. *FEBS J* 273: 4504−4515

Martinez-Sanz J, Kateb F, Assairi L, Blouquit Y, Bodenhausen G, Abergel D, Mouawad L, Craescu CT (2010) Structure, dynamics and thermodynamics of the human centrin 2/hSfi1 complex. *J Mol Biol* 395: 191−204

Middendorp S, Paoletti A, Schiebel E, Bornens M (1997) Identification of a new mammalian centrin gene, more closely related to *Saccharomyces cerevisiae* CDC31 gene. *Proc Natl Acad Sci USA* 94: 9141−9146

Middendorp S, Küntziger T, Abraham Y, Holmes S, Bordes N, Paintrand M, Paoletti A, Bornens M (2000) A role for centrin 3 in centrosome reproduction. *J Cell Biol* 148: 405−416

Nabais C, Peneda C, Bettencourt-Dias M (2020) Evolution of centriole assembly. *Curr Biol* 30: R494−R502

Nizak C, Martin-Lluesma S, Moutel S, Roux A, Kreis TE, Goud B, Perez F (2003) Recombinant antibodies against subcellular fractions used to track endogenous Golgi protein dynamics *in vivo*. *Traffic* 4: 739−753

Paoletti A, Moudjou M, Paintrand M, Salisbury JL, Bornens M (1996) Most of centrin in animal cells is not centrosome-associated and centrosomal centrin is confined to the distal lumen of centrioles. *J Cell Sci* 109: 3089−3102

Paoletti A, Bordes N, Haddad R, Schwartz CL, Chang F, Bornens M (2003) Fission yeast cdc31p is a component of the half-bridge and controls SPB duplication. *Mol Biol Cell* 14: 2793−2808

Prosser SL, Morrison CG (2015) Centrin2 regulates CP110 removal in primary cilium formation. *J Cell Biol* 208: 693−701

Rüthnick D, Vitale J, Neuner A, Schiebel E (2021) The N-terminus of Sfi1 and yeast centrin Cdc31 provide the assembly site for a new spindle pole body. *J Cell Biol* 220: e202004196

Salisbury JL, Baron A, Surek B, Melkonian M (1984) Striated flagellar roots: isolation and partial characterization of a calcium-modulated contractile organelle. *J Cell Biol* 99: 962−970

Sanders M, Salisbury J (1994) Centrin plays an essential role in microtubule severing during flagellar excision in *Chlamydomonas reinhardtii*. *J Cell Biol* 124: 795−805

Schindelin J, Arganda-Carreras I, Frise E, Kaynig V, Longair M, Pietzsch T, Preibisch S, Rueden C, Saalfeld S, Schmid B *et al* (2012) Fiji: an open-source platform for biological-image analysis. *Nat Methods* 9: 676−682

Schmidt TI, Kleylein-Sohn J, Westendorf J, Le Clech M, Lavoie SB, Stierhof Y-D, Nigg EA (2009) Control of centriole length by CPAP and CP110. *Curr Biol* 19: 1005−1011

Seybold C, Schiebel E (2013) Spindle pole bodies. *Curr Biol* 23: R858−R860

Spang A, Courtney I, Grein K, Matzner M, Schiebel E (1995) The Cdc31p-binding protein Kar1p is a component of the half bridge of the yeast spindle pole body. *J Cell Biol* 128: 863−877

Spektor A, Tsang WY, Khoo D, Dynlacht BD (2007) Cep97 and CP110 suppress a cilia assembly program. *Cell* 130: 678−690

Steib E, Laporte MH, Gambarotto D, Olieric N, Zheng C, Borgers S, Olieric V, Le Guennec M, Koll F, Tassin AM *et al* (2020) Wdr90 is a centriolar microtubule wall protein important for centriole architecture integrity. *Elife* 9: 1−28

Strnad P, Leidel S, Vinogradova T, Euteneuer U, Khodjakov A, Gönczy P (2007) Regulated HsSAS-6 levels ensure formation of a single procentriole per centriole during the centrosome duplication cycle. *Dev Cell* 13: 203−213

Takasaki Y, Deng JS, Tan EM (1981) A nuclear antigen associated with cell proliferation and blast transformation. *J Exp Med* 154: 1899−1909

Vallen EA, Ho W, Winey M, Rose MD (1994) Genetic interactions between CDC31 and KAR1, two genes required for duplication of the microtubule organizing center in *Saccharomyces cerevisiae*. *Genetics* 137: 407−422

Wolfrum U, Salisbury JL (1998) Expression of centrin isoforms in the mammalian retina. *Exp Cell Res* 242: 10−17

Expanded View Figures

Figure EV1. SFI1 localization at centrioles revealed by expansion microscopy.

A   Representative confocal image of expanded U2OS centrioles stained with α/β-tubulin (αβTub, magenta) and SFI1 (green, home-made antibody). White arrowheads point to the SFI1 signal at mature centrioles and white arrows highlight the SFI1 signal at procentrioles. M stands for mature centrioles and P for Procentrioles. Scale bar: 200 nm.

B   Representative confocal image of expanded RPE-1 centrioles stained for α/β-tubulin (αβTub, magenta) and SFI1 (green, home-made antibody). Arrowheads point to the SFI1 signal at mature centrioles while the thin arrows highlight the SFI1 signal at procentrioles. M stands for mature centrioles and P for procentrioles. Scale bar: 200 nm.

C, D   Representative confocal image of expanded RPE-1 centrioles treated with siCT (C) or siSFI1 (D), stained with α/β-tubulin (αβTub, magenta) and SFI1 (green, home-made antibody). White arrowheads point to the SFI1 signal at the distal end of centrioles while red arrowhead points to a faint proximal signal. Scale bar: 200 nm.

E   Relative SFI1 intensity in the indicated conditions showing a significant decrease in siSFI1-treated cells.

F   Representative confocal image of expanded U2OS centrioles stained with α/β-tubulin (αβTub, magenta) and SFI1 (green, commercial antibody). White arrowheads point to the SFI1 signal at mature centrioles and white arrows highlight the SFI1 signal at procentrioles. M stands for mature centrioles and P for procentrioles. Scale bar: 200 nm.

G   Representative confocal image of expanded RPE-1 centrioles stained for α/β-tubulin (αβTub, magenta) and SFI1 (green, commercial antibody). White arrowheads indicate the SFI1 signal at mature centrioles and white arrows highlight the SFI1 signal at procentrioles. M stands for mature centriole and P for procentriole. Scale bar: 200 nm.

H–K   Representative confocal image of expanded RPE-1 centrioles treated with siCT (H, I) or siSFI1 (J, K), stained with α/β-tubulin (αβTub, magenta) and SFI1 (green, commercial antibody). White arrowheads point to SFI1 signal at the distal end of centrioles while red arrowhead points to a faint proximal signal. Scale bars: 200 nm (H, J) and 100 nm (I, K).

L, M   Representative widefield images of expanded centrioles from U2OS cells treated with siSFI1. Cells are stained for α/β-tubulin (αβTub, magenta) and SFI1 (green) allowing the quantification of the siSFI1 efficiency which can lead to either total SFI1 depletion (No SFI1, L) or incomplete SFI1 depletion (Partial SFI1, M).

N–P   Representative widefield images of expanded U2OS centrioles treated with siCT or siPOC5, stained with α/β-tubulin (αβTub, magenta) and POC5 (green, N), Cetn2/3 (green, O) or SFI1 + POC5 (green, P). White arrowheads indicate the remaining proximal belt of POC5 sometimes observable in siPOC5 treated cells when depletion is incomplete (N, middle panel). Note that Centrin behavior seems to follow POC5 upon POC5 depletion (O, middle panel). Asterisks indicate the presence of the distal dot of Centrin and SFI1 in POC5-depleted cells. Scale bar: 200 nm.

Q   Quantification of the siPOC5 efficiency at centrosomes.

R   Percentage of depleted centrioles (without POC5 staining) containing SFI1 as a distal dot in siCT and siPOC5 treated cells.

Data information: Average ± SD, N, statistical analysis: (E) siCT (area under the curve): 0.79 ± 0.2, siSFI1 (area under the curve): 0.55 ± 0.3. N = 24 for siCT and 50 for siSFI1 from 4 independent experiments. Mann–Whitney test (***P < 0.0001). (Q) siCT = 96.4% ± 5.4; siPOC5 = 43.8% ± 11.6, N = 5 independent experiments (100 cells/experiment). Mann–Whitney test (**P = 0.002). (R) siCT = 94.5% ± 6.4; siPOC5 = 92.5% ± 6.4. N = 2 independent experiments (100 cells/experiment). Mann–Whitney test (P = 0.667).
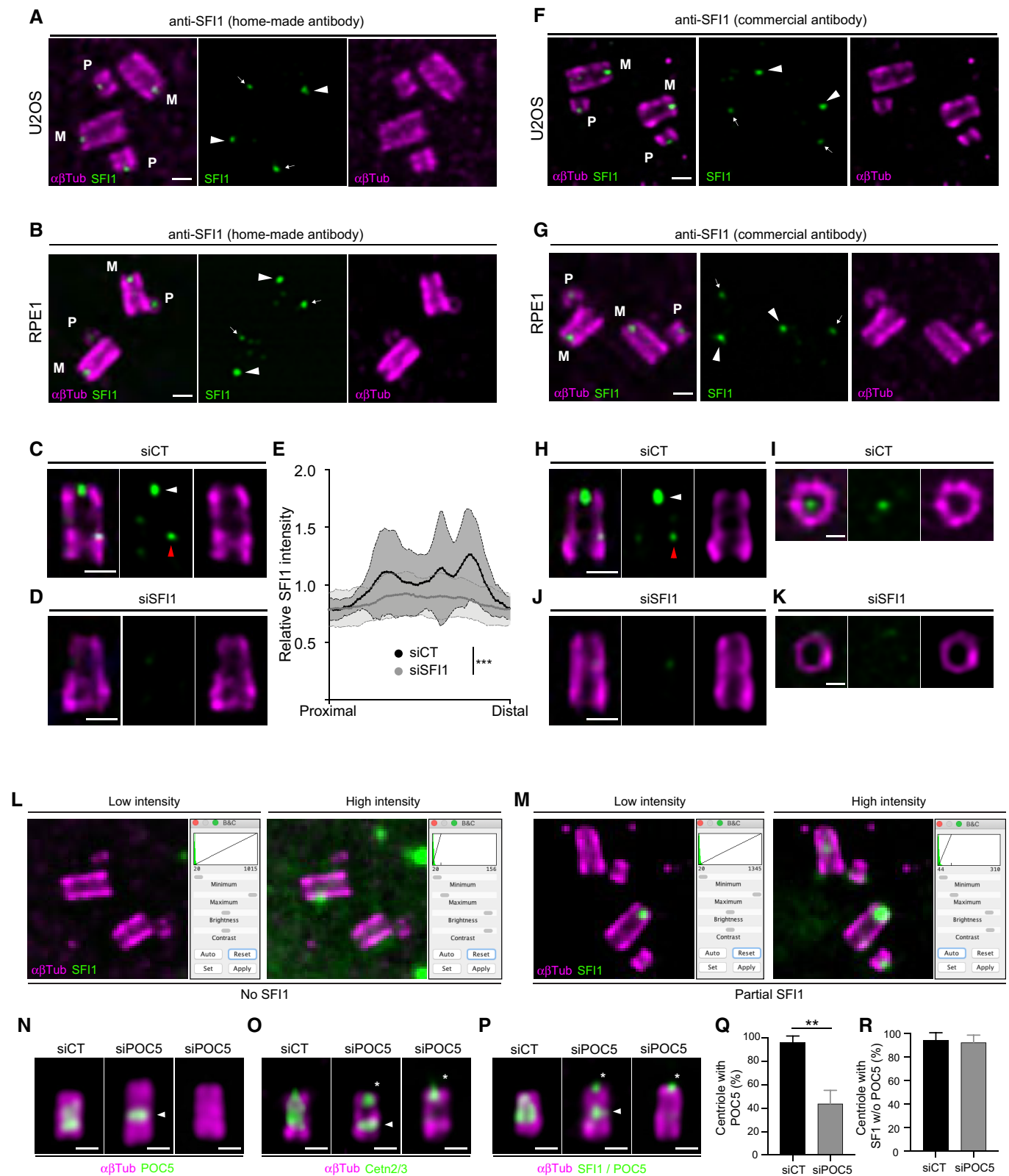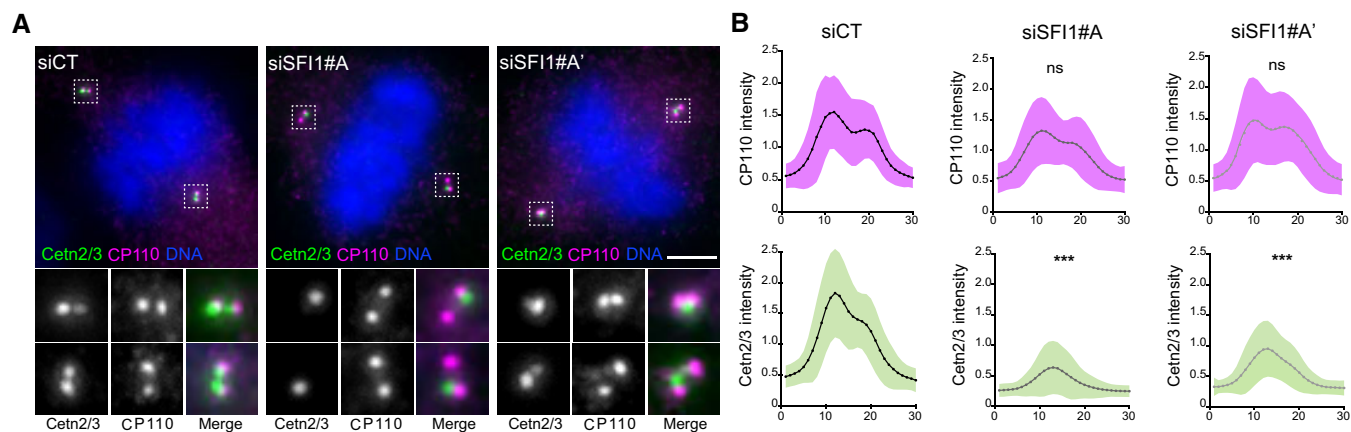
Figure EV1.

Figure EV2. **SFI1 depletion alters centriolar Centrin position but not CP110.**

A   Representative confocal images of mitotic control and SFI1-depleted RPE1-1 cells stained for Centrin (Cetn2/3, green) and CP110 (magenta). Scale bar: 5 μm.
B   CP110 (magenta) and Centrin (green) relative integrated intensities from a plot profile across the 2 centrioles in control and SFI1-depleted cells (siSFI1#A and siSFI1#A′ correspond to two different siRNAs, see material and methods). Average ± SD, *N*, statistical analysis: siCT (area under the curve) = CP110: 1 ± 0.3, Cetn2/3: = 0.99 ± 0.5. siSFI1#A (area under the curve) = CP110: 0.9 ± 0.3, Cetn2/3: 0.4 ± 0.1. siSFI1#A′ (area under the curve) = CP110: 1 ± 0.3, Cetn2/3: 0.5 ± 0.2. *N* = 60 cells from three independent experiments. Unpaired *t*-test (***P < 0.0001).

Figure EV3. Characterization of SFI1 depletion in HeLa and U2OS.

A, B   Representative widefield images of expanded centrioles from HeLa cells treated with siCT or siSFI1#A. Cells are stained with Tubulin (magenta) and SFI1 (green, A) or Cetn2/3 (gray, B). Yellow asterisks show the absence of SFI1 (A) and Cetn2/3 (B) at the distal tip of the centriole in siSFI1-treated cells. Scale bar: 250 nm. Quantifications show the similar loss of SFI1 and Cetn2/3 in SFI1-depleted cells.

C   Representative widefield images of expanded centrioles from HeLa cells treated siSFI1#A and stained for tubulin (magenta) and SFI1 (green). Note the abnormal shape and structural alteration of the centriole in SFI1-depleted cells. Yellow asterisks show the absence of SFI1. Red arrowheads indicate abnormal centrioles. Scale bar: 250 nm.

D   Quantification of the percentage of duplicating centrioles in the indicated conditions.

E   Percentage of abnormal centrioles in the indicated conditions.

F, G   Representative widefield images of expanded centrioles from HeLa cells treated with siCT or siSFI1#B. Cells are stained with Tubulin (magenta) and SFI1 (green, F) or Cetn2/3 (gray, G). Yellow asterisks show the decreased intensity of SFI1 (F) and Cetn2/3 (G) at the distal tip of the centriole in siSFI1-treated cells. Scale bar: 250 nm.

H   Quantification of the efficiency of the siSFI1 shows a mild loss of SFI1 in these conditions.

I   Quantification of the percentage of duplicating centrioles in the indicated conditions.

J   Percentage of abnormal centrioles in the indicated conditions.

K, L   Quantification of the signal intensities of SFI1 (K) and Cetn2/3 (L) in HeLa cells treated with siCT or siSFI1#B showing a marked decrease of both SFI1 and Cetn2/3 at the level of mature and procentriole. However, the complete disappearance of the signal was rarely observed (see panel H).

M, N   Representative widefield images of expanded centrioles from U2OS cells treated with siCT or siSFI1#B. Cells are stained for tubulin (magenta) and SFI1 (green, M) or Cetn2/3 (gray, N). Yellow asterisks show the decreased intensity of SFI1 (M) and Cetn2/3 (N) at the distal tip of the centriole in siSFI1-treated cells. Scale bar: 250 nm.

O   Quantification of the efficiency of the siSFI1 shows a mild loss of SFI1 in these conditions.

P   Quantification of the percentage of duplicating centrioles in the indicated conditions.

Q   Percentage of abnormal centrioles in the indicated conditions.

R, S   Quantification of the signal intensities of SFI1 (R) and Cetn2/3 (S) in U2OS cells treated with siCT or siSFI1#B showing a notable decrease of both SFI1 and Cetn2/3 at the level of mature and procentriole. However, the complete disappearance of the signal was rarely observed (see panel O).

Data information: Average $\pm$ SD, *N*, statistical analysis: (A) siCT = Intact SFI1: 97.2% $\pm$ 3.9, Partial SFI1: 2.8% $\pm$ 3.9, No SFI1: 0% $\pm$ 0, siSFI1 = Intact SFI1: 11.3% $\pm$ 7.6, Partial SFI1: 32.2% $\pm$ 12.6, No SFI1: 56.5% $\pm$ 5. *N* = 2 independent experiments (> 50 centrioles per experiment). Two-way ANOVA (***P < 0.0001). (B) siCT = Intact Cetn2/3: 95% $\pm$ 7.1, Partial Cetn2/3: 5% $\pm$ 7.1, No Cetn2/3: 0% $\pm$ 0, siSFI1 = Intact Cetn2/3: 14.4% $\pm$ 14.9, Partial Cetn2/3: 36.2% $\pm$ 8.7, No Cetn2/3: 49.4% $\pm$ 6.3. *N* = 2 independent experiments (> 50 centrioles per experiment). Two-way ANOVA (***P < 0.0001). (D) siCT: 49.9% $\pm$ 7, siSFI1#A: 60.7 $\pm$ 6.8. *N* = 3 independent experiments (> 50 cells/experiment). Unpaired *t*-test (P = 0.13). (E) siCT: 2.1% $\pm$ 1.9, siSFI1#A: 21.1% $\pm$ 2.6. *N* = 3 independent experiments (> 50 cells/experiment). Unpaired *t*-test (***P = 0.0005). (H) siCT = Intact SFI1: 97.4% $\pm$ 4.4, Partial SFI1: 2.6% $\pm$ 4.4, No SFI1: 0% $\pm$ 0, siSFI1 = Intact SFI1: 84.9% $\pm$ 4.3, Partial SFI1: 15.1% $\pm$ 4.3, No SFI1: 0% $\pm$ 0. *N* = 3 independent experiments (> 50 centrioles per experiment). Two-way ANOVA (***P = 0.0002). (I) siCT: 47.6% $\pm$ 2.2, siSFI1#B: 57.1 $\pm$ 6.8. *N* = 3 independent experiments (> 50 centrioles per experiment). Unpaired *t*-test (P = 0.08). (J) siCT: 1.2% $\pm$ 2.3, siSFI1#B: 2.3 $\pm$ 2.3. *N* = 3 independent experiments (> 50 centrioles per experiment). Unpaired *t*-test (P = 0.63). (K) siCT mature: 1.0 $\pm$ 0.13, siSFI1#B mature: 0.69 $\pm$ 0.06, siCT procentriole: 1.0 $\pm$ 0.10, siSFI1#B procentriole: 0.70 $\pm$ 0.10. *N* = 58, 47, 45, 57 for siCT mature, siSFI1#B mature, siCT procentriole and siSFI1#B procentriole respectively, from three independent experiments. One-way ANOVA (***P < 0.0001 in all conditions). (L) siCT mature: 1.0 $\pm$ 0.12, siSFI1#B mature: 0.69 $\pm$ 0.13, siCT procentriole: 1.0 $\pm$ 0.12, siSFI1#B procentriole: 0.70 $\pm$ 0.07. *N* = 37, 34, 37, 40 for siCT mature, siSFI1#B mature, siCT procentriole and siSFI1#B procentriole respectively, from three independent experiments. One-way ANOVA (***P < 0.0001 in all conditions). (O) siCT = Intact SFI1: 100% $\pm$ 0, Partial SFI1: 0% $\pm$ 0, No SFI1: 0% $\pm$ 0, siSFI1#B=Intact SFI1: 86.2% $\pm$ 1.5, Partial SFI1: 12.5% $\pm$ 1.6, No SFI1: 2% $\pm$ 2.8. *N* = 3 independent experiments (> 50 centrioles per experiment). Two-way ANOVA (***P = 0.0001). (P) siCT: 44.1% $\pm$ 4.7, siSFI1#B: 51.8 $\pm$ 3.3. *N* = 3 independent experiments (> 50 centrioles per experiment). Unpaired *t*-test (P = 0.08). (Q) siCT: 1.1% $\pm$ 1.2, siSFI1#B: 1.3 $\pm$ 1.5. *N* = 3 independent experiments (> 50 centrioles per experiment). Unpaired *t*-test (P = 0.86). (R) siCT mature: 1.0 $\pm$ 0.10, siSFI1#B mature: 0.70 $\pm$ 0.09, siCT procentriole: 1.0 $\pm$ 0.11, siSFI1#B procentriole: 0.70 $\pm$ 0.08. *N* = 100, 83, 74, and 57 for siCT mature, siSFI1#B mature, siCT procentriole, and siSFI1#B procentriole respectively, from three independent experiments. One-way ANOV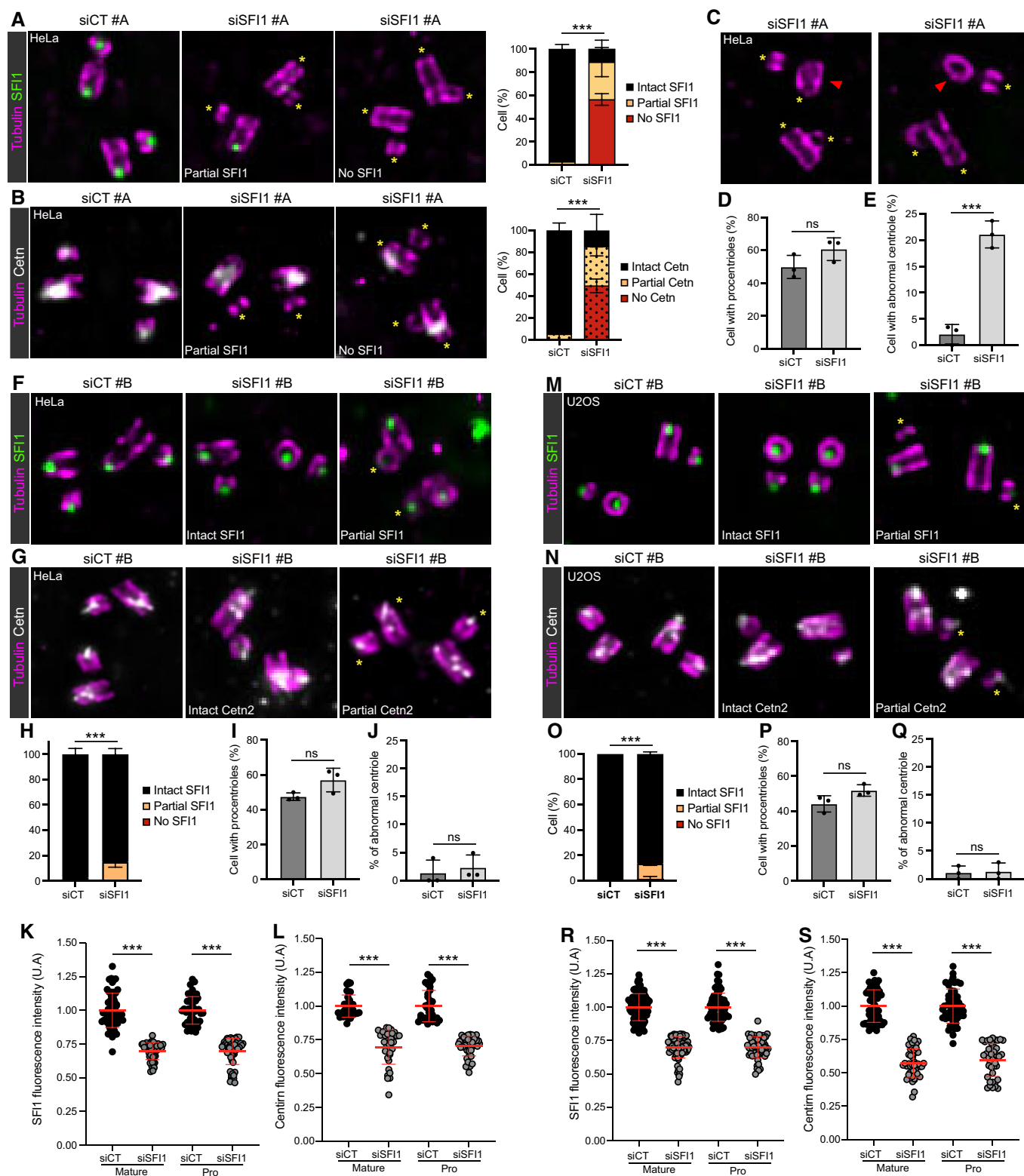A (***P < 0.0001 in all conditions). (S) siCT mature: 1.0 $\pm$ 0.12, siSFI1#B mature: 0.58 $\pm$ 0.11, siCT procentriole: 1.0 $\pm$ 0.13, siSFI1#B procentriole: 0.60 $\pm$ 0.12. *N* = 58, 48, 51, 41 for siCT mature, siSFI1#B mature, siCT procentriole, and siSFI1#B procentriole respectively, from three independent experiments. One-way ANOVA (***P < 0.0001 in all conditions).

Figure EV3.

Figure EV4. Gallery of defective centrioles in SFI1-depleted RPE-1 cells.

A, B   Confocal images of expanded centrioles from SFI1-depleted RPE-1 stained for α/β-tubulin (magenta). Top view (top panel) and side view (bottom panels) of broken centriole (A) and abnormal but not broken (B) stained for (α/β-tubulin, magenta) and SFI1 (green). Scale bar: 200 nm.

C, D   Confocal images of expanded centrioles from SFI1-depleted RPE-1 stained for α/β-tubulin (magenta) and CP110 (yellow). Top view (top panel) and side view (bottom panels) of broken centriole (C) and abnormal but not broken (D) stained for (α/β-tubulin, magenta) and CP110 (yellow). Scale bar: 200 nm.
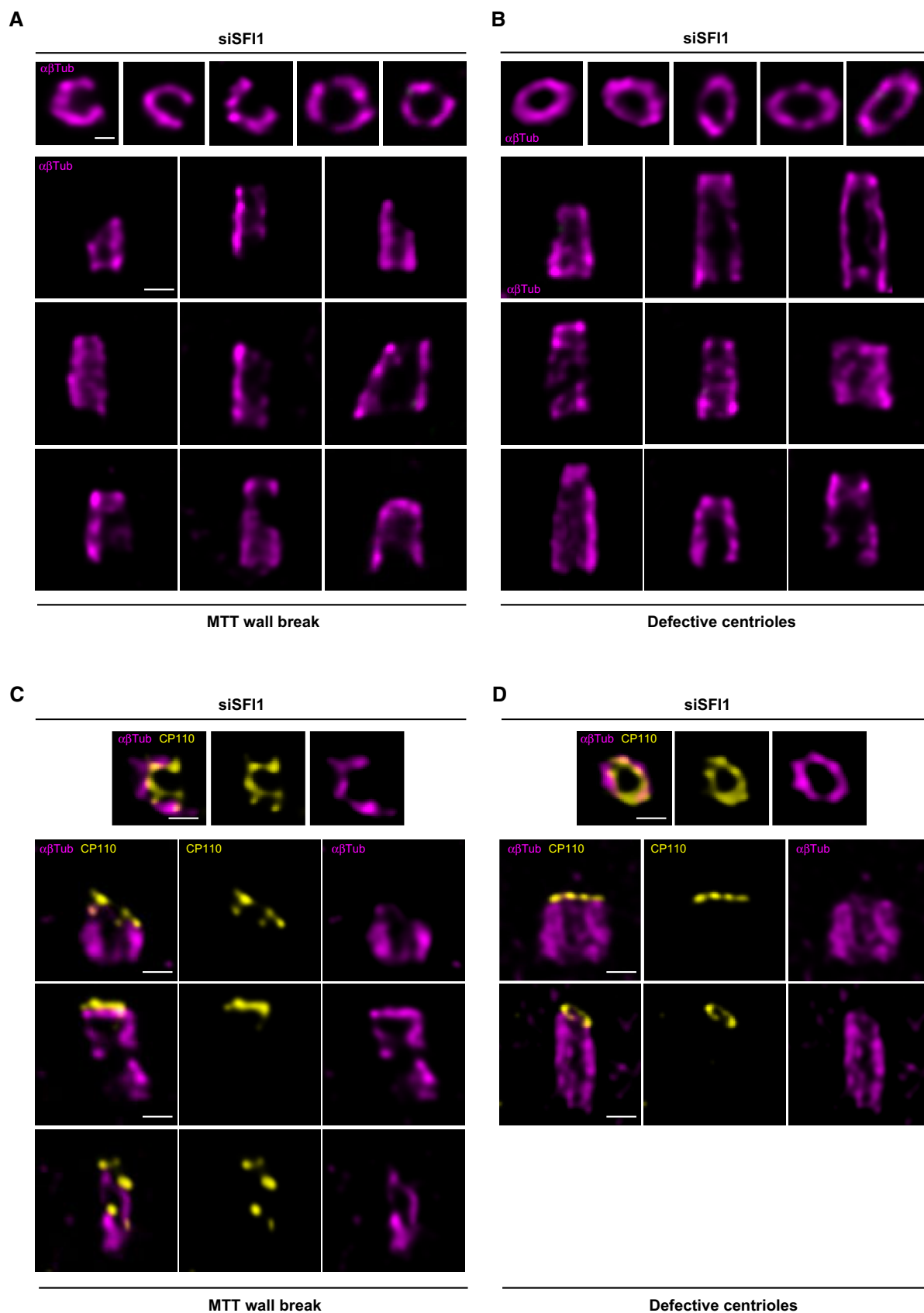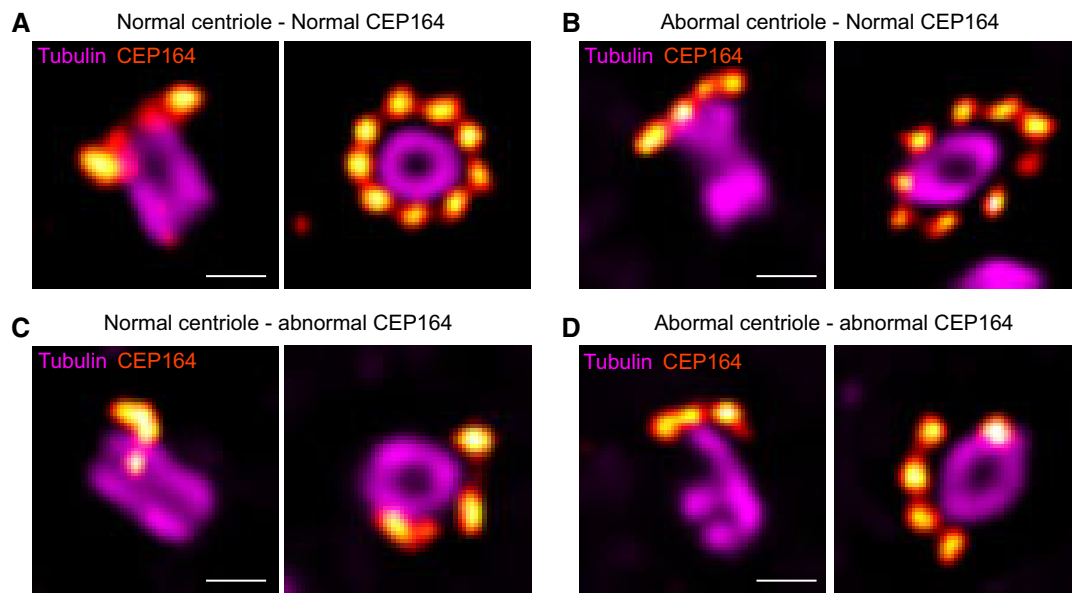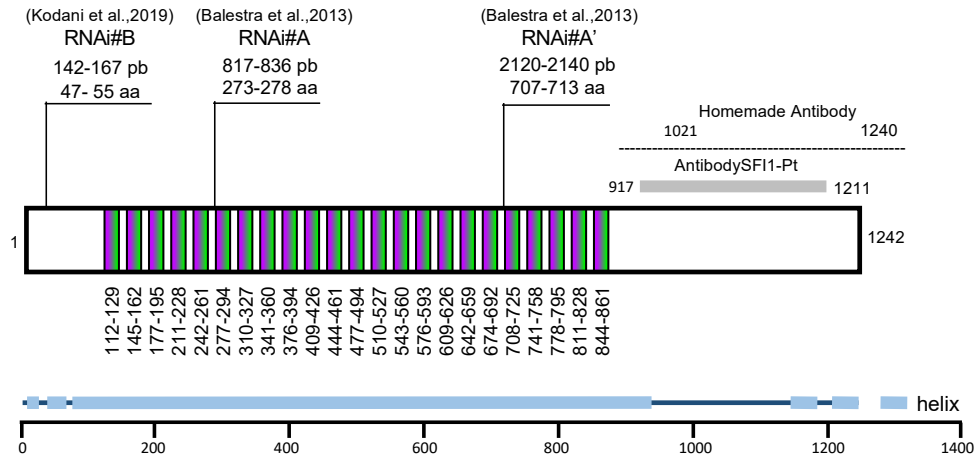
Figure EV4.

Figure EV5. CEP164 disorganization in SFI1-depleted RPE-1.

A–D Representative widefield images of expanded centrioles in siSFI1-depleted cells stained for tubulin (magenta) and CEP164 (red hot). Each panel shows a different combination of alterations such as normal centriole with normal CEP164 (A), abnormal centriole with normal CEP164 (B), normal centriole with abnormal CEP164 (C), and abnormal centriole with abnormal CEP164 (D). Scale bars: 250 nm.

23 repeats

MKNLLTEKCISSHNFHQKVIKQRMEKKVDSRYFKDGAVKKPYSAKTLSNKKSSASFGIRRELPSTSHLV
QYRGTHTCTRQGRLRELRIRCVARKFLYLWIRMTFGRVFPSKARFYYEQRLLRKVFEEWKEEWWVFQ
HEWKLCVRADCHYRYYLYNLMFQTWKTYVRQQQEMRNKYIRAEVHDAKQKMRQAWKSWLIYVVVRR
TKLQMQTTALEFRQRIILRVWWSTWRQRLGQVRVSRALHASALKHRALSLQVQAWSQWREQLLYVQK
EKQKVVSAVKHHQHWQKRRFLKAWLEYLQVRRVKRQQNEMAERFHHVTVLQIYFCDWQQAWERRE
SLYAHHAQVEKLARKMALRRAFTHWKHYMLLCAEEAAQFEMAEEHHRHSQLYFCFRALKDNVTHAHL
QQIRRNLAHQQHGVTLLHRFWNLWRSQIEQKKERELLPLLHAAWDHYRIALLCKCIELWLQYTQKRRYK
QLLQARADGHFQQRALPAAFHTWNRLWRWRHQENVLSARATRFHRETLEKQVFSLWRQKMFQHRE
NRLAERMAILHAERQLLYRSWFMWHQQAAARHQEQEWQTVACAHHRHGRLKKAFCLWRESAQGLRT
ERTGRVRAAEFHMAQLLRWAWSQWRECLALRGAERQKLMRADLHHQHSVLHRALQAWVTYQGRVR
SILREVAARESQHNRQLLRGALRRWKENTMARVDEAKKTFQASTHYRRTICSKVLVQWREAVSVQMY
YRQQEDCAIWEAQKVLDRGCLRTWFQRWWDCSRRSAQQRLQLERAVQHHHRQLLLEGLARWKTHH
LQCVRKRLLHRQSTQLLAQRLSRTCFRQWRQQLAARRQEQRATVRALWFWAFSLQAKVWATWLAFV
LERRRKKARLQWALQAYQGQLLQEGATRLLRFAASMKSRQQLQAQQQVQAAHSLHRAVRRCATLWK
QKVLGRGGKPQPLAAIAPSRKVTFEGPLLNRIAAGAGDGTLETKRPQASRPLGALGRLAAEEPHALELN
TAHSARKQPRRPHFLLEPAQSQRPQKPQEHGLGMAQPAAPSLTRPFLAEAPTALVPHSPLPGALSSAP
GPKQPPTASTGPELLLLPLSSFMPCGAAAPARVSAQRATPRDKPPVPSSLASVPDPHLLLPGDFSATRA
GPGLSTAGSLDLEAELEEIQQQLLHYQTTKQNLWSCRRQASSLRRWLELNREEPGPEDQEVEQQVQK
ELEQVEMQIQLLAEELQAQRQPIGACVARIQALRQALC

Appendix Figure S1. Human SFI1 protein. Schematic representation of the 1242 amino acid human SFI1 protein. Note the relative position of the two antibodies used in this study (home-made antibody and SFI1-Pt, Proteintech) as well as the regions targeted by the three siRNAs used in this study. As both siRNA#A and siRNA#A' (from Balestra et al.,) gave similar results, only the siRNA#A was used throughout the manuscript. The 23 SFI1 repeats are underlined. The colors magenta, cyan and green highlight the SFI1 motif.
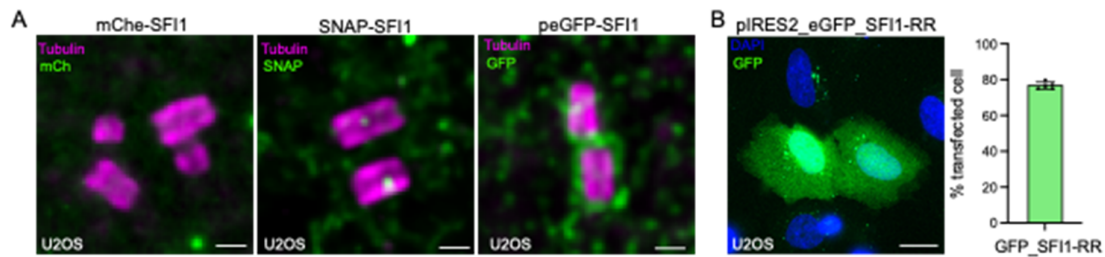
Appendix Figure S2. SFI1 rescue experiment strategies. (**A**). Representative widefield images of expanded centrioles from U2OS transfected with mCherry-SFI1 (green, left), SNAP-Sfi1 (green, middle) and peGFP-SFI1 (green, right) showing an absence (mChe-SFI1, SNAP-SFI1) or incorrect (peGFP-SFI1) localization of SFI1 at the centriole (Tubulin, magenta). Scale bar: 250 nm (**B**). Representative widefield image of U2OS cells transfected with pIRES_eGFP_SFI1-RR plasmid. Scale bar: 20 µm. Quantification shows the transfection efficiency (78.2% +/- 2.8).
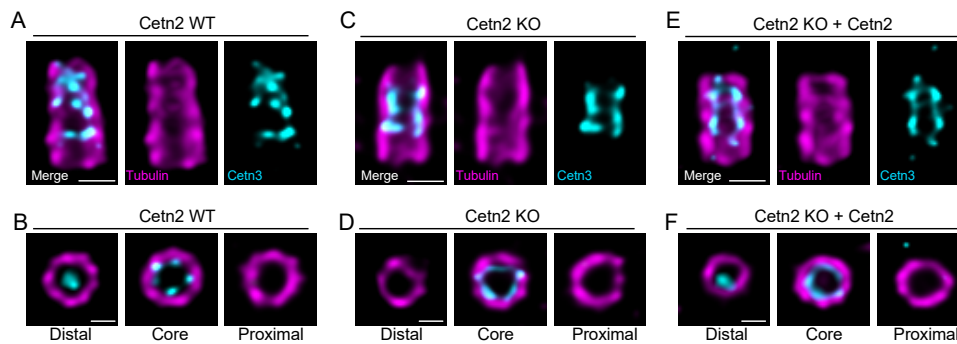
Appendix Figure S3. Distal Centrin 3 is lost in Centrin 2 KO RPE-1 cells. Representative confocal images of expanded side-viewed (**A**, **C**, **E**) and top-viewed (**B**, **D**, **F**) centrioles from Centrin 2 WT (**A**, **B**), Centrin 2 KO (**C**, **D**) and Centrin 2 KO rescued with Centrin 2 (**E**, **F**) cells. Cells are stained for α/β-tubulin (magenta) and Centrin 3 (cyan) showing the loss of the distal dot of Centrin 3, but not the core, in Centrin 2 KO cells. Note that the re-expression of Centrin 2 in Centrin 2 KO cells rescues the distal position of Centrin 3. Scale bars : 200 nm (**A, C, E**) and 100 nm (**B, D, F**).